

Magnon-mediated quantum gates for superconducting qubits

Martijn Dols,^{1,2,*} Sanchar Sharma,³ Lenos Bechara,¹ Yaroslav M. Blanter,² Marios Kounalakis,^{1,2,4,†} and Silvia Viola Kusminskiy^{1,5,‡}

¹*Institute for Theoretical Solid State Physics, RWTH Aachen University, 52074 Aachen, Germany*

²*Kavli Institute of Nanoscience, Delft University of Technology, 2628 CJ Delft, The Netherlands*

³*Laboratoire de Physique de l'École Normale Supérieure, ENS, Université PSL, CNRS, Sorbonne Université, Université de Paris, F-75005 Paris, France*

⁴*Luxembourg Institute of Science & Technology, 4422 Belvaux, Luxembourg*

⁵*Max Planck Institute for the Science of Light, Staudtstraße 2, 91058 Erlangen, Germany*

(Dated: June 24, 2024)

We propose a hybrid quantum system consisting of a magnetic particle inductively coupled to two superconducting transmon qubits, where qubit-qubit interactions are mediated via magnons. We show that the system can be tuned into three different regimes of effective qubit-qubit interactions, namely a transverse ($XX + YY$), a longitudinal (ZZ) and a non-trivial ZX interaction. In addition, we show that an enhanced coupling can be achieved by employing an ellipsoidal magnet, carrying anisotropic magnetic fluctuations. We propose a scheme for realizing two-qubit gates, and simulate their performance under realistic experimental conditions. We find that iSWAP and CZ gates can be performed in this setup with an average fidelity $\gtrsim 99\%$, while an iCNOT gate can be applied with an average fidelity $\gtrsim 88\%$. Our proposed hybrid circuit architecture offers an alternative platform for realizing two-qubit gates between superconducting qubits and could be employed for constructing qubit networks using magnons as mediators.

I. INTRODUCTION

Hybrid quantum systems provide a promising route towards practical applications by combining the advantages of different platforms for quantum information tasks [1, 2]. For example, superconducting (SC) qubits make excellent processors for quantum computing [3–5]. Quantum gates for SC qubits can be performed within several nanoseconds [6–8], with fidelities exceeding 99%, as required for the error correction schemes of surface codes [9–11]. However, the dissipation rates of SC qubits make them impractical for long-term data storage, imposing the need for integration with more appropriate physical systems in order to construct quantum memories [1, 2]. Furthermore, SC circuits do not couple directly to optical photons, which is an important requirement for building quantum networks [1, 2]. Therefore, there is a practical need for bridging systems of diverse nature and functionality.

Magnons, the collective excitations of ordered spin systems, have shown promising properties to operate as such mediators [12–14], owing to their capability of coupling coherently to various excitations, e.g. optical photons [15–19], microwaves [20–24], phonons [25–30], and spins [31–33]. These couplings can be further enhanced using magnetization squeezing [34], which can be implemented using anisotropically shaped magnetic structures [35]. Moreover, by considering insulating magnetic materials, such as the paradigmatic Yttrium Iron Garnet (YIG), magnon dissipation channels can be minimized

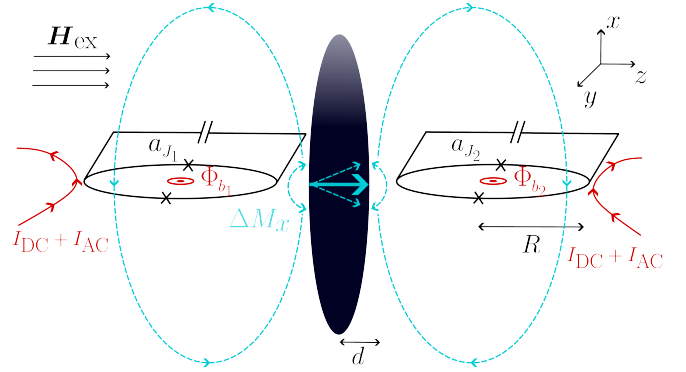


FIG. 1: Proposed setup consisting of two transmon qubits inductively coupled via their SQUID loop to a YIG ellipsoid. The ground state of the magnetization is along the z axis due to the external magnetic field $\mathbf{H}_{\text{ex}} = H_0 \mathbf{e}_z$. The magnetic quantum fluctuations, ΔM_x , of the YIG ellipsoid in the x direction induce a flux in each SQUID loop, thereby modulating the inductance of both qubits and resulting in an effective qubit-qubit coupling mediated by magnons. Two dedicated flux bias lines, carrying DC and AC current, are used to control the flux in each loop.

[36]. These properties suggest that magnons can be useful for mediating the coupling between different types of qubits, e.g. in spin-based or SC-based platforms. The coupling of magnons to SC transmon qubits has been indeed experimentally demonstrated via mediating microwave cavities [37–40]. Furthermore, it has been proposed that coherent coupling between a transmon qubit and a YIG sphere can also be achieved by the dipolar fields in free space, resulting in an interaction that can

* martijn.dols@rwth-aachen.de

† marios.kounalakis@gmail.com

‡ kusminskiy@physik.rwth-aachen.de

be tuned between a radiation-pressure and an exchange type [41]. This interaction can, for example, be employed in order to control and entangle magnons in distant YIG spheres, using the qubit as a mediator and bypassing the need for microwave cavities [42].

In this work, we extend this framework by exploring the possibility of using magnons as mediators to couple SC qubits in free space. Various methods have been demonstrated to couple qubits to each other directly, including capacitive [7, 43–45] and inductive [46–50] coupling. Alternatively, a cavity bus or other qubits can be employed to mediate the coupling [51–54]. These schemes focus on either direct coupling via circuit elements or indirect coupling via other circuit modes. Adding magnons to the list of possible mediators can open up new directions in qubit-qubit coupling schemes, e.g. by harnessing chiral coupling [55, 56]. We show that, using magnons as virtual mediators of a tunable qubit-qubit interaction, a set of quantum gates can be realized with different degrees of fidelity which we characterize and optimize. Specifically, we propose a hybrid quantum system consisting of two flux-tunable transmon qubits coupled via a magnet. We consider a magnet with an anisotropic shape, which can enhance the coupling strength. We find that, by appropriately choosing the SC qubit parameters, three different types of effective qubit-qubit interactions can be realized: $XX + YY$, ZZ , and ZX . We use these to simulate three two-qubit gates, namely an iSWAP gate, a controlled-Z (CZ) gate and an iCNOT gate, respectively. Using experimentally realistic parameters for the setup, we obtain average gate fidelity values $\gtrsim 99\%$ for the iSWAP and CZ gate, and $\gtrsim 88\%$ for the iCNOT gate. The combination of any of these two-qubit gates with single-qubit rotations forms a universal gate set [57, 58].

The remainder of this manuscript is structured as follows. In Sec. II we review the theory of flux-tunable transmon qubits coupled to an anisotropic magnet leading to squeezing of the relevant quadrature of the magnetization fluctuations. In Sec. III we derive the different regimes of magnon-mediated qubit-qubit interaction giving rise to the corresponding gates, and compare the performance of the dissipative system against the ideal case by defining a gate-fidelity measure. In Sec. IV we present the conclusions and discuss possibilities for improving the average gate fidelity values. Some details of the calculations have been relegated to the Appendix.

II. MODEL AND COUPLING

We consider two flux-tunable SC transmon qubits coupled to a magnet of an anisotropic shape as depicted in Fig. 1. A flux-tunable transmon qubit [59] consists of a superconducting quantum interference device (SQUID) made of an SC loop with two Josephson junctions with Josephson energies E_J^1 and E_J^2 , shunted by a capacitor C with charging energy $E_C = e^2/(2C)$. An im-

portant parameter is the SQUID asymmetry, given by $a_J = |E_J^1 - E_J^2|/E_J^\Sigma$, where $E_J^\Sigma = E_J^1 + E_J^2$. Applying current through a nearby external bias line induces a flux Φ_b into the SQUID loop. We define the reduced flux as $\varphi_b = \pi\Phi_b/\Phi_0$, where $\Phi_0 = h/(2e)$ is the magnetic flux quantum. The transmon Hamiltonian reads [59]

$$\hat{H}_Q = 4E_C\hat{n}^2 - E_J^\Sigma S(\varphi_b) \cos(\hat{\varphi}), \quad (1)$$

where \hat{n} corresponds to the number of Cooper pairs participating in tunnelling, $S(\varphi_b) = \sqrt{\cos^2(\varphi_b) + a_J^2 \sin^2(\varphi_b)}$, and $\hat{\varphi} = \hat{\delta} - \arctan(a_J \tan(\varphi_b))$ is the SC phase difference. We consider the transmon regime $E_J^\Sigma S(\varphi_b) \gg E_C$, in which the qubit becomes insensitive to charge noise [59]. Expanding the cosine and introducing the annihilation and creation operators \hat{c} and \hat{c}^\dagger ,

$$\hat{n} = i\frac{\epsilon}{2}(\hat{c}^\dagger - \hat{c}), \quad \hat{\varphi} = \frac{1}{\epsilon}(\hat{c}^\dagger + \hat{c}) \quad (2)$$

with $\epsilon^4 = E_J^\Sigma S(\varphi_b)/(2E_C)$, one obtains [59]

$$\hat{H}_Q = \hbar\omega_q\hat{c}^\dagger\hat{c} - \frac{E_C}{2}\hat{c}^\dagger\hat{c}^\dagger\hat{c}\hat{c}, \quad (3)$$

where we defined the transmon frequency $\omega_q = (\sqrt{8E_C E_J^\Sigma S(\varphi_b)} - E_C)/\hbar$. The non-linearity of the second term in Eq. (3) results in anharmonic energy levels, which is a necessary condition for the construction of a qubit [60].

For the magnet we consider an ellipsoidal shape of dimensions $L_x \gg L_y = L_z$, where L_i is the length of the semi axis of the magnet in the i -th direction (see Fig. 1) and $V_m = 4\pi L_x L_z^2/3$ its volume. An external homogeneous magnetic field is applied along the z axis, $\mathbf{H}_{\text{ex}} = H_0 \mathbf{e}_z$. This field fulfills $H_0 > M_s/2$ such that the classical ground state of the magnet is $\mathbf{M} = M_s \mathbf{e}_z$, where M_s is the saturation magnetization. The shape anisotropy favors fluctuations of the magnetization along the x direction, implying that the quantum fluctuations of the ground state $|0\rangle_m$, denominated a *squeezed vacuum*, are anisotropic [61]. In what follows we consider only the magnon excitations associated with the uniform precession of the spins, called Kittel magnons. Within the linear spin wave approximation they are described by

$$\hat{H}_M = \hbar\omega_m\hat{m}^\dagger\hat{m}, \quad (4)$$

where $\hat{m}^{(\dagger)}$ are the magnon annihilation (creation) operators operating on the squeezed vacuum such that $\hat{m}|0\rangle_m = 0$, and the frequency is given by [35]

$$\omega_m = \mu_0\gamma H_0 \sqrt{1 - \frac{M_s}{H_0}(3N_T - 1)}. \quad (5)$$

Here, N_T is a dimensionless factor of the demagnetization tensor which depends on the shape of the magnet [62, 63].

For $L_x \gg L_z$ as considered in this work we have $N_T \approx \frac{1}{2}$ [63]. In the isotropic case $N_T = 1/3$ and the Kittel mode frequency for a spherical magnet, independent of demagnetization factors, is recovered.

Fluctuations of the magnetization, which are proportional to $1/\sqrt{V_m}$ [35], give rise to fluctuations of the magnetic dipole moment $\Delta\hat{\boldsymbol{\mu}}$,

$$\Delta\hat{\mu}_x = \mu_{\text{zpf}} e^r (\hat{m} + \hat{m}^\dagger), \quad \Delta\hat{\mu}_y = i\mu_{\text{zpf}} e^{-r} (\hat{m} - \hat{m}^\dagger). \quad (6)$$

Here, $\mu_{\text{zpf}} = \hbar\gamma_0\sqrt{N_s/2}$ is the value of the isotropic zero point fluctuations with γ_0 the modulus of the gyromagnetic ratio, $N_s = \rho_s V_m$ the total number of spins, and ρ_s the spin density. Magnets with volumes greater than 100 nm^3 and typical YIG spin densities [37] obey $N_s \gg 1$. Since $\Delta\hat{\mu}_z/\mu_{\text{zpf}} \propto 1/N_s$, we can neglect the z fluctuations of the magnetic moment [64]. The factor r is the *squeezing parameter* and satisfies [35]

$$e^r = \left(1 - \frac{M_s}{H_0}(3N_T - 1)\right)^{-\frac{1}{4}}. \quad (7)$$

In the limit $H_0 \rightarrow (3N_T - 1)M_s$, the magnon frequency ω_m vanishes, see Eq. (5), and the squeezing parameter r diverges. In this case, $\Delta\hat{\mu}_x$ exponentially diverges with r , whereas $\Delta\hat{\mu}_y$ is suppressed. In practice, however, achievable cryogenic temperatures and the stability of the magnetically ordered ground state for these values of H_0 impose a lower bound on ω_m , and therefore an upper bound on squeezing [35].

We consider the magnet positioned between the qubits as shown in Fig. 1. The magnetic field due to the fluctuations $\Delta\hat{\boldsymbol{\mu}}$ induces a flux through the SQUID loop

$$\Phi(\Delta\hat{\boldsymbol{\mu}}) = \frac{\mu_0}{4\pi} \sum_{i=x,y} I_i \Delta\hat{\mu}_i, \quad (8)$$

where μ_0 is the magnetic constant and I_i are geometrical factors which have the dimension of 1/length. Due to the symmetry of the chosen setup one finds $I_y = 0$. The geometrical factor I_x is the largest for SQUID loops which are positioned at the $x = 0$ plane and increases as d (the minimal distance between the center of the magnet and the SQUID loop) decreases. A lower bound on d is imposed by the critical field that the SC wire can support [64]. To determine I_x , we use the field of an ellipsoid [65]; see details in App. A. We find $I_x = -0.1/\mu\text{m}$ for $L_x/L_z \approx 4$. The stray magnetic field of the magnet is about two orders of magnitude lower than the critical field of typical superconductors [66], as we elaborate in App. A.

The flux bias φ_b can be controlled by the magnetic field generated by the wires carrying electric currents as shown in Fig. 1. The reduced flux caused by $\Delta\hat{\boldsymbol{\mu}}$ is given by

$$\varphi(\Delta\hat{\boldsymbol{\mu}}) = \frac{\mu_0 I_x \mu_{\text{zpf}} e^r}{4\Phi_0} (\hat{m}^\dagger + \hat{m}). \quad (9)$$

Replacing $\varphi_b \rightarrow \varphi_b + \varphi(\Delta\hat{\boldsymbol{\mu}})$ in Eq. (1) and considering flux fluctuations much smaller than φ_b gives the interaction Hamiltonian $\hat{H}_{\text{int}} = \hat{H}_J + \hat{H}_g$ [41]. The first term is a coherent exchange interaction between a qubit and the magnons

$$\hat{H}_J = \hbar J (\hat{c}^\dagger \hat{m} + \hat{c} \hat{m}^\dagger)$$

with the coupling constant

$$J = -\frac{\mu_0 I_x \mu_{\text{zpf}} a_J e^r}{4\Phi_0} \left(\frac{2E_C (E_J^\Sigma)^3}{S(\varphi_b)^5} \right)^{\frac{1}{4}}, \quad (10)$$

while the second term is given by

$$\hat{H}_g = \hbar g \hat{c}^\dagger \hat{c} (\hat{m}^\dagger + \hat{m})$$

with the coupling strength

$$g = -\frac{\mu_0 I_x \mu_{\text{zpf}} e^r}{8\Phi_0} \left(\frac{2E_C E_J^\Sigma}{S(\varphi_b)^3} \right)^{\frac{1}{2}} \sin(2\varphi_b) (1 - a_J^2). \quad (11)$$

This second interaction term resembles an optical photon-magnon coupling [17] or radiation pressure in optomechanical systems [67]. Note that, because of the enhanced fluctuations of the magnetic moment $\Delta\hat{\mu}_x$ due to squeezing, the coupling strengths J and g are enhanced by e^r .

The total Hamiltonian of the system with two SC qubits therefore reads

$$\hat{H}_{\text{tot}} = \hat{H}_0 + \hat{H}_{\text{int}}, \quad (12)$$

where

$$\hat{H}_0 = \hat{H}_M + \sum_{i=1,2} \hat{H}_T^i, \quad (13)$$

with \hat{H}_M the magnon Hamiltonian given by Eq. (4), and

$$\hat{H}_T^i = \hbar\omega_{q_i} \hat{c}_i^\dagger \hat{c}_i - \frac{E_C}{2} \hat{c}_i^\dagger \hat{c}_i^\dagger \hat{c}_i \hat{c}_i \quad (14)$$

is the Hamiltonian for each SC qubit labeled by $i \in \{1, 2\}$. The interaction term between the SC qubits and the magnon mode is given by

$$\hat{H}_{\text{int}} = \sum_{i=1,2} \hat{H}_J^i + \hat{H}_g^i, \quad (15)$$

with

$$\hat{H}_J^i = \hbar J_i (\hat{c}_i^\dagger \hat{m} + \hat{c}_i \hat{m}^\dagger) \quad (16)$$

and

$$\hat{H}_g^i = \hbar g_i \hat{c}_i^\dagger \hat{c}_i (\hat{m}^\dagger + \hat{m}), \quad (17)$$

where the coupling constants of the magnons to each qubit can be tuned independently and are given by Eqs. (10) and (11).

III. QUANTUM GATES

The Hamiltonian \hat{H}_{tot} can be brought into the form of an effective qubit-qubit interaction up to second order in the coupling constants J_i and g_i by performing a Schrieffer-Wolff (SW) transformation, as we show in Appendix C. The effective interaction allows us to identify the coupling parameters that are required in order to realize different gates by appropriately tuning the coupling constants. These can be tuned by controlling the SQUID asymmetry a_J (which is a design parameter) for each qubit, and the reduced flux φ_b . We identify two limiting cases: (i) for symmetric SQUIDs, $a_J = 0$, where the coupling strength $J = 0$, following Eq. (10), and (ii) for a highly asymmetric SQUID with $a_J \rightarrow 1$ and a value of the reduced flux $\varphi_b = \pi/2$, where the coupling constant g vanishes according to Eq. (11). In Appendix C we show that combinations of these limiting cases give rise to the three gates studied in this section: iSWAP, CZ and iC-NOT. In what follows we characterize the performance of the gate generated by the Hamiltonian \hat{H}_{tot} of Eq. (12) for the parameter regime of each gate (which we denote by \hat{H}_{gate}) and in the presence of dissipation, compared to the ideal gate associated with the corresponding effective qubit-qubit Hamiltonian.

In order to take into account the dissipative evolution of the system we use a Liouvillian description. Depending on the gate, we apply a specific Hamiltonian \hat{H}_{gate} and hence a specific Liouvillian $\mathcal{L}_{\text{gate}}$. The time evolution of the density matrix of the composite system $\hat{\rho}_c$, describing both qubits and the magnon field, can be found by solving the Lindblad master equation $\frac{d}{dt}\hat{\rho}_c(t) = \mathcal{L}_{\text{gate}}[\hat{\rho}_c(t)]$, where

$$\mathcal{L}_{\text{gate}}[\hat{\rho}_c] = -\frac{i}{\hbar} \left[\hat{H}_{\text{gate}}, \hat{\rho}_c \right] + \sum_{n=1}^6 \left(\hat{L}_n \hat{\rho}_c \hat{L}_n^\dagger - \frac{1}{2} \left\{ \hat{L}_n^\dagger \hat{L}_n, \hat{\rho}_c \right\} \right). \quad (18)$$

Here, \hat{L}_n are the Lindblad operators. Magnon damping is taken into account by $\hat{L}_1 = \sqrt{\kappa(1+n_{\text{th}})}\hat{m}$, where κ is the magnon linewidth and the bosonic expectation number $n_{\text{th}} = (\exp[\hbar\omega_m/(k_B\mathcal{T})] - 1)^{-1}$, with k_B as the Boltzmann factor and \mathcal{T} as the temperature. The linewidth is known from experiments to have the form $\kappa = \alpha_G\omega_m + \tilde{\kappa}$ [68–70], where α_G is the Gilbert damping and $\tilde{\kappa}$ is the inhomogeneous damping. The thermal excitation of magnons is given by $\hat{L}_2 = \sqrt{\kappa n_{\text{th}}}\hat{m}^\dagger$. For the qubits we include the decay of the transmons with $\hat{L}_3 = \sqrt{1/T_1}\hat{c}_1$ and $\hat{L}_4 = \sqrt{1/T_1}\hat{c}_2$, where T_1 is the qubit lifetime, and pure dephasing terms $\hat{L}_5 = \sqrt{1/T_\phi}\hat{c}_1^\dagger\hat{c}_1$ and $\hat{L}_6 = \sqrt{1/T_\phi}\hat{c}_2^\dagger\hat{c}_2$, where T_ϕ is the dephasing time.

We assume for simplicity that initially the magnons are prepared in the vacuum state, and we describe the two-qubit space by the density matrix $\hat{\rho}$. This assumption does not affect significantly our results as long as the initial thermal occupation is low, as we discuss in

Sec. III B. We propagate the initial state until an appropriately chosen gate time T_{gate} at which the desired gate is applied. After the time propagation, the magnons are traced-out, since we are solely interested in the qubit dynamics. In summary, we consider the following quantum channel,

$$\mathcal{E}_{\text{gate}}[\hat{\rho}] = \text{Tr}_m \left[e^{\mathcal{L}_{\text{gate}}T_{\text{gate}}} [\hat{\rho} \otimes |0\rangle\langle 0|_m] \right]. \quad (19)$$

To quantify how well $\mathcal{E}_{\text{gate}}$ simulates a given gate \hat{U}_{gate} , we determine the average gate fidelity given by $\bar{F}(\mathcal{E}_{\text{gate}}, \hat{U}_{\text{gate}})$ where \bar{F} is defined as [71]

$$\bar{F}(\mathcal{E}, \hat{U}) = \int d\psi \langle \psi | \hat{U}^\dagger \mathcal{E}[\psi] \langle \psi | \hat{U} | \psi \rangle. \quad (20)$$

Here, one integrates over the uniform measure $d\psi$, which is normalized such that $\int d\psi = 1$. This integral can be simplified to a finite summation over a unitary basis [71], as we elaborate in Appendix B.

One can find the SW transformed Hamiltonian with general qubit levels in Appendix C. In order to find the gate times which come from the effective qubit-qubit coupling and to identify the frame in which the gate is performed, we limit the qubits of these effective Hamiltonians to their energetically lowest two levels in the next sections. One can recognize Hamiltonians in the two-level approximation by the usage of the Pauli operators: $\hat{\sigma}^+ = |1\rangle\langle 0|$, $\hat{\sigma}^- = |0\rangle\langle 1|$, and $\hat{\sigma}^z = |1\rangle\langle 1|$. In simulations we use Hamiltonians which do not involve truncated qubit levels and are written in terms of the ladder operators \hat{c}_i and \hat{c}_i^\dagger . We summarize the strategy applied to evaluate the different gates in Fig. 2.

A. iSWAP

For highly asymmetric SQUIDs with $a_{J_1}, a_{J_2} \rightarrow 1$ and reduced flux $\varphi_{b_1}, \varphi_{b_2} = \pi/2$ we have $g_1, g_2 \rightarrow 0$. We obtain the effective qubit-qubit interaction for these parameters from \hat{H}_{tot} as detailed in Appendix C 1. We find

$$\begin{aligned} \hat{H}_{\text{SW}}^{\text{iSWAP}} = & \hbar \left(\omega_m - \sum_{i=1,2} \frac{J_i^2}{\omega_{q_i} - \omega_m} \right) \hat{m}^\dagger \hat{m} \\ & + \sum_{i=1,2} \hbar \left(\omega_{q_i} + \frac{J_i^2}{\omega_{q_i} - \omega_m} \right) \hat{\sigma}_i^z \\ & + \hbar g_S (\hat{\sigma}_1^+ \hat{\sigma}_2^- + \hat{\sigma}_1^- \hat{\sigma}_2^+), \end{aligned} \quad (21)$$

with the effective qubit-qubit coupling constant

$$g_S = \frac{J_1 J_2}{2} \left(\frac{1}{\omega_{q_1} - \omega_m} + \frac{1}{\omega_{q_2} - \omega_m} \right). \quad (22)$$

We note that besides the exchange-like induced qubit-qubit coupling term, the interaction induces a Stark shift of the frequencies ω_m and ω_{q_i} . This transformation is valid for $J_i \ll \omega_{q_i} - \omega_m$, i.e. in the dispersive regime.

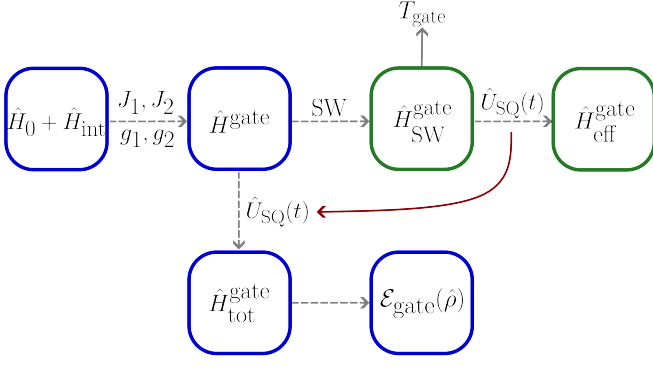


FIG. 2: Visual summary of the method used to obtain the quantum channel $\mathcal{E}_{\text{gate}}[\rho]$. A given set of coupling constants J_1, J_2, g_1 and g_2 yields the total Hamiltonian for a particular gate, \hat{H}^{gate} . With a SW transformation we obtain an approximate qubit-qubit Hamiltonian $\hat{H}_{\text{SW}}^{\text{gate}}$, where the effective coupling strength dictates the gate time T_{gate} . We cancel single-qubit rotations with a unitary transformation $\hat{U}_{\text{SQ}}(t)$ to obtain the effective Hamiltonian $\hat{H}_{\text{eff}}^{\text{gate}}$. We apply this unitary transformation to the initial Hamiltonian as well to find $\hat{H}_{\text{tot}}^{\text{gate}}$. We use this final Hamiltonian to construct the quantum channel, which we use in our simulations. For the system Hamiltonians indicated by blue boxes, all quantum levels are included in the analysis, whereas green boxes indicate that the two-level approximation is applied.

Time propagation of the coupling term of the Hamiltonian of Eq. (21) for a time $T_S = \pi/(2|g_S|)$ gives an iSWAP gate: $\exp(-ig_S T_S (\hat{\sigma}_1^+ \hat{\sigma}_2^- + \hat{\sigma}_1^- \hat{\sigma}_2^+)) = \hat{U}_{\text{iSWAP}}$, where we defined

$$\hat{U}_{\text{iSWAP}} = \frac{1}{2} (\hat{I} \otimes \hat{I} \mp i \hat{\sigma}_x \otimes \hat{\sigma}_x \mp i \hat{\sigma}_y \otimes \hat{\sigma}_y + \hat{\sigma}_z \otimes \hat{\sigma}_z). \quad (23)$$

Here, $\hat{\sigma}_x, \hat{\sigma}_y$ and $\hat{\sigma}_z$ are the Pauli matrices. This gate swaps $|01\rangle \leftrightarrow |10\rangle$ while adding a phase $\mp i$ and leaves the symmetrical states $|00\rangle$ and $|11\rangle$ untouched. The sign of the phase $\mp i$ corresponds to $g_S \gtrless 0$.

The second term of Eq. (21) causes the qubits to undergo rotations on top of the interaction. We assume for simplicity identical qubits, so that $J = J_1 = J_2$ and $\omega_q = \omega_{q_1} = \omega_{q_2}$. A unitary transformation with

$$\hat{U}_{\text{SQ}}(t) = \exp \left[it \left(\omega_q + \frac{J^2}{\omega_q - \omega_m} \right) \left(\hat{m}^\dagger \hat{m} + \sum_{i=1,2} \hat{\sigma}_i^z \right) \right] \quad (24)$$

cancels these phase rotations yielding

$$\begin{aligned} \hat{H}_{\text{eff}}^{\text{iSWAP}} &= \hat{U}_{\text{SQ}} \hat{H}_{\text{SW}}^{\text{iSWAP}} \hat{U}_{\text{SQ}}^\dagger + i\hbar \frac{d\hat{U}_{\text{SQ}}}{dt} \hat{U}_{\text{SQ}}^\dagger \\ &= \hbar \left(\omega_m - \omega_q - \frac{3J^2}{\omega_q - \omega_m} \right) \hat{m}^\dagger \hat{m} \\ &\quad + \hbar g_S (\hat{\sigma}_1^+ \hat{\sigma}_2^- + \hat{\sigma}_1^- \hat{\sigma}_2^+). \end{aligned} \quad (25)$$

In order to cancel the single-qubit rotations at the level of the original Hamiltonian, we apply this transformation

to \hat{H}_{tot} , which yields

$$\begin{aligned} \hat{H}_{\text{tot}}^{\text{iSWAP}} &= \hbar \left(\omega_m - \omega_q - \frac{J^2}{\omega_q - \omega_m} \right) \hat{m}^\dagger \hat{m} \\ &\quad - \sum_{i=1,2} \left(\frac{\hbar J^2}{\omega_q - \omega_m} \hat{c}_i^\dagger \hat{c}_i + \frac{E_C}{2} \hat{c}_i^\dagger \hat{c}_i^\dagger \hat{c}_i \hat{c}_i \right) \\ &\quad + \sum_{i=1,2} \hbar J (\hat{c}_i^\dagger \hat{m} + \hat{c}_i \hat{m}^\dagger). \end{aligned} \quad (26)$$

We use this Hamiltonian to obtain the channel $\mathcal{E}_{\text{iSWAP}}[\rho]$ and compare it to the ideal iSWAP gate given by Eq. (23), by computing the average gate fidelity as a function of the magnon frequency, see Eq. (20). The result is shown in Fig. 3(a).

We see that the average fidelity is a non-monotonic function of the magnon frequency, which is a consequence of two competing factors affecting the effective coupling strength g_S and therefore the gate time T_S . Minimizing the gate time is important in order to minimize the effect of dissipation and hence to improve the gate fidelity. On the one hand, Eq. (22) shows that g_S is enhanced as the magnon frequency approaches the resonance condition $\omega_m = \omega_q$. This is reflected in Fig. 3(a), where the gate time T_S goes to zero when approaching $\omega_m/\omega_q = 1$. Note however that, as this resonance is approached, the SW transformation used to obtain the ideal gate breaks down (signaled by a diverging coupling g_S) so that the effective, ideal-gate Hamiltonian is not a good approximation to the total one at this point. Physically, a resonant magnon-qubit coupling causes real magnonic excitations (as opposed to the virtual ones in the off-resonant case) which adversely affect the gate fidelity. This causes the rapid decrease of the average gate fidelity as the resonance is approached. On the other hand, the coupling strength is enhanced by magnon squeezing. As Eq. (22) shows, the coupling is proportional to $J_1 J_2$ and hence $g_S \propto e^{2r}$. In order to have $e^r \gg 1$ the magnon frequencies are required to be small $\omega_m \ll \gamma \mu_0 M_s$, which corresponds to the far left side of Fig. 3(a). At such low frequencies, however, magnonic thermal excitations are important, decreasing the gate fidelity. The effect of squeezing around the qubit frequency region is generally negligible due to $e^r \approx 1$. This competition of effects gives rise to the maximum of the average gate fidelity at low frequencies.

For the results shown in Fig. 3 we set $a_J = 0.9$ for both qubits, considering fabrication constraints [75] and in order to maintain the frequency tunability [41]. The reduced flux of both qubits is set to $\varphi_b = \pi/2$ such that $g_1 = g_2 = 0$, in agreement with the considered iSWAP regime. We assume typical transmon energies $E_C/h = 150$ MHz and $E_J^\Sigma/h = 35$ GHz, such that the qubit frequency is $\omega_q/(2\pi) = 6.0$ GHz [76]. In the simulations we use Fock spaces with size 3 for the qubits and 4 for the magnons [77]. A maximal fidelity of $\bar{F} = 99.00\%$ is obtained at $\omega_m/\omega_q = 0.94$. For this magnon frequency the effective qubit-qubit coupling is $g_S/\omega_q = 8.2 \times 10^{-5}$

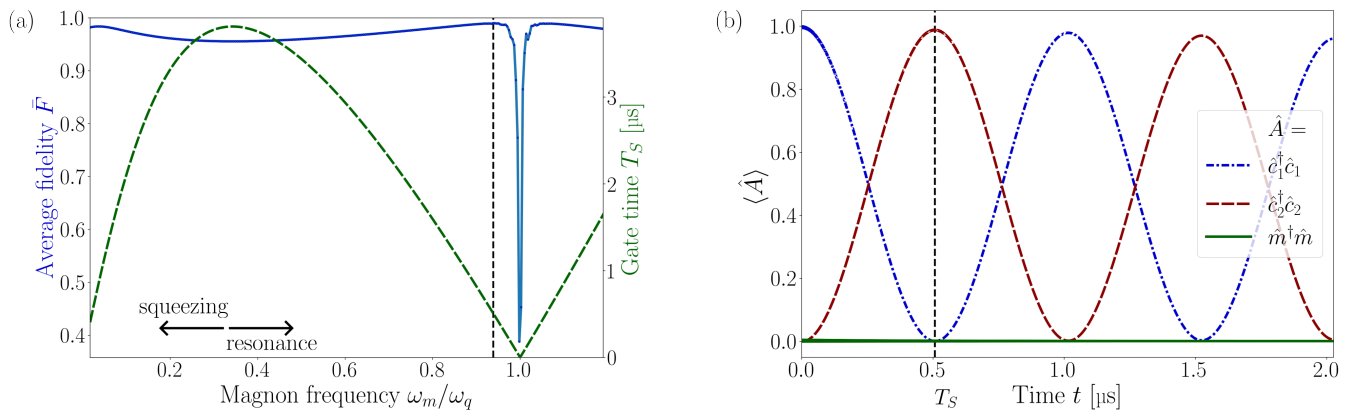


FIG. 3: (a) Average fidelity \bar{F} (blue, solid) and gate time T_S (green, dashed) for the iSWAP gate as a function of the magnon frequency ω_m in units of the SC qubit frequencies $\omega_q = \omega_{q_1} = \omega_{q_2}$. T_S drops at low frequencies due to the squeezing enhancement of the qubit-qubit coupling strength g_S , and approaches 0 for $\omega_m/\omega_q \rightarrow 1$ due to the resonant enhancement of g_S . Undesired magnonic excitations near resonance and thermal excitations at low frequencies cause the average fidelity to drop. The maximum fidelity is $\bar{F} = 99.00\%$ at $\omega_m/\omega_q = 0.94$ (vertical dashed line). (b) Qubit and magnon dynamics following the evolution with the Hamiltonian of Eq. (26) in the presence of dissipation at the optimal magnon frequency $\omega_m = 0.94\omega_q$. The input state is $|\psi\rangle = |10\rangle$. The occupation of both qubits (blue, dash-dotted and red, dashed) and magnons (green, solid) as a function of time t are shown. In this regime, the magnon occupation remains ~ 0 at all times. The gate time $T_S = 0.5 \mu\text{s}$ is indicated with a vertical dashed line, at which the target state equals $\hat{U}_{\text{iSWAP}}|\psi\rangle = -i|01\rangle$. Parameters: $L_x = 16 \mu\text{m}$, $L_z = 3.9 \mu\text{m}$, $R = 25 \mu\text{m}$, $d - L_z = 10 \text{nm}$, $\alpha_G = 10^{-4}$, $\tilde{\kappa}/(2\pi) = 0.1 \text{MHz}$ [68–70] and $\mathcal{T} = 10 \text{mK}$, $T_1 = 100 \mu\text{s}$ and $T_\phi = 100 \mu\text{s}$ [72–74].

corresponding to $g_S/(2\pi) = 0.49 \text{MHz}$ for the parameters used.

In Fig. 3(b) we show the dynamics of the system including dissipation for a given input state, $|10\rangle$ and for a magnon frequency tuned to the optimal average fidelity. From $t = 0$ to $t = T_S$, which corresponds to the dashed line, the swap takes place. We see that the excitation of the first qubit is transferred to the second qubit, as we expect from $\hat{U}_{\text{iSWAP}}|10\rangle = -i|01\rangle$, whereas the magnon occupation remains close to zero as expected for virtual transitions.

In order to turn off the qubit-qubit coupling once the gate has been realized at the gate time T_S , the interaction term in Eq. (21) can be made off resonant by detuning the qubits. This can be achieved by varying the reduced flux bias φ_b . Simulations show that changing the reduced flux of one qubit to $\varphi_b = \pi/3$ while keeping the other at $\varphi_b = \pi/2$ is sufficient.

The configuration described above can also be used to construct a $\sqrt{\text{iSWAP}}$ gate by choosing a gate time $T_S/2$. This gate can be used to create Bell-like states, such as $|01\rangle - i|10\rangle$ [78]. In our setup, using the same parameters as in Fig. 3, we find that such a state can be prepared with an average gate fidelity $\bar{F} = 99.54\%$.

B. CZ

In the case of symmetric SQUIDs with $a_{J_1}, a_{J_2} \rightarrow 0$, we have $J_1, J_2 \rightarrow 0$. In this case we obtain the following

effective interaction Hamiltonian (see App. C 2)

$$\hat{H}_{\text{SW}}^{\text{CZ}} = \hbar\omega_m \hat{m}^\dagger \hat{m} + \sum_{i=1,2} \hbar \left(\omega_{q_i} - \frac{g_i^2}{\omega_m} \right) \hat{\sigma}_i^z - \hbar g_Z \hat{\sigma}_1^z \hat{\sigma}_2^z, \quad (27)$$

where the effective coupling strength is given by

$$g_Z = \frac{2g_1 g_2}{\omega_m}. \quad (28)$$

This transformation is valid for $g_i \ll \omega_m$. At $T_Z = \pi/g_Z$, the coupling term in Eq. (27) results in a CZ gate, since $\exp(ig_Z T_Z \hat{\sigma}_1^z \hat{\sigma}_2^z) = \hat{U}_{\text{CZ}}$, where we defined

$$\hat{U}_{\text{CZ}} = |0\rangle\langle 0| \otimes \hat{I} + |1\rangle\langle 1| \otimes \hat{\sigma}_z. \quad (29)$$

If either of the qubits is excited, a Pauli gate $\hat{\sigma}_z$ is applied on the target qubit.

The second term of the transformed Hamiltonian (27) causes qubit rotations regardless of the state of the control qubit. We cancel these with the unitary transformation

$$\hat{U}_{\text{SQ}}(t) = \exp \left[it \left(\sum_{i=1,2} \left(\omega_{q_i} - \frac{g_i^2}{\omega_m} \right) \hat{\sigma}_i^z \right) \right]. \quad (30)$$

This yields

$$\hat{H}_{\text{eff}}^{\text{CZ}} = \hbar\omega_m \hat{m}^\dagger \hat{m} - \hbar g_Z \hat{\sigma}_1^z \hat{\sigma}_2^z \quad (31)$$

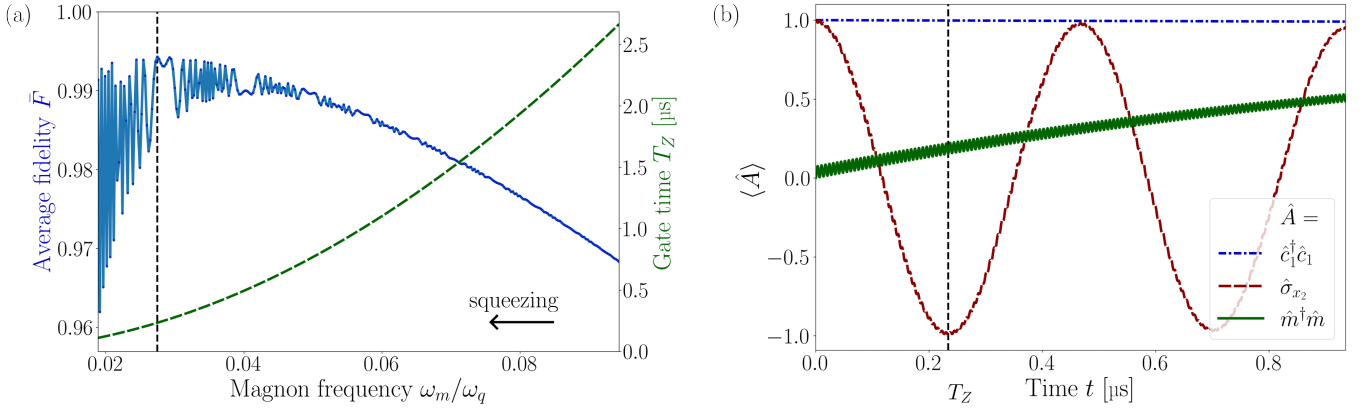


FIG. 4: (a) Average fidelity \bar{F} (blue, solid) and gate time T_Z (green, dashed) of the CZ gate as a function of the magnon frequency ω_m in units of the qubit frequencies ω_q . A competition between squeezing enhancement of the coupling g_Z and thermal occupation at low frequencies results in a maximum fidelity $\bar{F} = 99.43\%$ at $\omega_m/\omega_q = 0.027$ (vertical dashed line). The oscillatory behavior for low magnon frequencies is due to a resonant enhancement of the parametric interaction between magnons and qubits, causing an oscillating magnon occupation, see also green solid line in (b). (b) Demonstration of the proposed CZ gate for a given input state ($|1+\rangle$) at the optimal magnon frequency $\omega_m = 0.027\omega_q$. We plot the occupation of qubit 1 (blue, dash-dotted) and of the magnons (green, solid) as a function of time. In addition, we plot the evolution of the expectation value of the Pauli $\hat{\sigma}_x$ operator for the second qubit (red, dashed). The target state, achieved at $T_Z = 0.23\ \mu\text{s}$ (vertical dashed line), equals $\hat{U}_{CZ}|1+\rangle = |1-\rangle$. Parameters as in Fig. 3.

for the effective Hamiltonian and

$$\begin{aligned} \hat{H}_{\text{tot}}^{\text{CZ}} = & \hbar\omega_m \hat{m}^\dagger \hat{m} + \sum_{i=1,2} \frac{\hbar g_i^2}{\omega_m} \hat{c}_i^\dagger \hat{c}_i \\ & + \sum_{i=1,2} \hbar g_i \hat{c}_i^\dagger \hat{c}_i (\hat{m}^\dagger + \hat{m}). \end{aligned} \quad (32)$$

when applied to \hat{H}_{tot} with $J_1 = J_2 = 0$. We substitute the total Hamiltonian of Eq. (32) into the quantum channel $\mathcal{E}_{CZ}[\hat{\rho}]$, which we use in the optimization of the average gate fidelity and which we compare to the CZ gate in Eq. (29), as displayed in Fig. 4(a).

As discussed before, we aim to minimize the gate time in order to limit the effect of dissipation on the gate performance. Unlike the iSWAP gate, the coupling constant does not depend on the qubit frequency. Both squeezing and the $1/\omega_m$ proportionality of the coupling constant benefit from low magnon frequencies, so that the gate time improves as the magnon frequency decreases as Fig. 4(a) shows. Thermal occupation at low frequencies, in turn, leads to a decrease of the average fidelity as for the iSWAP gate, see Fig. 3(a) for comparison, leading to a maximum of the average gate fidelity. As the magnon frequency is decreased, the parametric interaction term between magnons and qubits is resonantly enhanced (see Eq. (32)), causing a small oscillating magnon occupation as seen in Fig. 4(b). The amplitude of these oscillations depends on the magnon frequency, resulting in the oscillations of the average fidelity as a function of frequency in Fig. 4(a), with increasing amplitude for lower frequencies.

In order to obtain the results depicted in Fig. 4 we set

$a_J = 0$ and $\varphi_b = \pi/4$ for both qubits corresponding in this case to $\omega_q/(2\pi) = 5.3$ GHz. We increased the Fock space size of the magnons to 6. We find an optimal average gate fidelity of $\bar{F} = 99.43\%$ for $\omega_m/\omega_q = 0.027$. This corresponds to $g_Z/\omega_q = 4.0 \times 10^{-4}$ ($g_Z/(2\pi) = 2.1$ MHz), a thermal expectation number $n_{\text{th}} = 1$ and a squeezing enhancement of $e^r = 4.2$.

The time dynamics of the proposed gate is illustrated in Fig. 4(b) for the input state $|1+\rangle = |1\rangle \otimes (|0\rangle + |1\rangle)/\sqrt{2}$. For simplicity we take the first qubit to be the control qubit. Since this qubit is in the excited state, a $\hat{\sigma}_z$ is applied to the target qubit according to Eq. (29). This gives $\hat{\sigma}_z |+\rangle = (|0\rangle - |1\rangle)/\sqrt{2} = |-\rangle$. Due to $\hat{\sigma}_x |+\rangle = |+\rangle$ and $\hat{\sigma}_x |-\rangle = -|-\rangle$, we find that the expectation value of the second qubit changes from 1 at $t = 0$ to -1 at $t = T_Z$, as Fig. 4(b) confirms.

The proposed gate of Eq. (19) assumes vacuum as the initial state for the magnons. Since the thermal expectation number is $n_{\text{th}} \sim 1$ for the optimal magnon frequency we found, a protocol for magnon cooling would need to be introduced in order to prepare the initial state into the ground state. To circumvent this necessity, we checked the performance of a gate using instead an initial magnon thermal state with $n_{\text{th}} = 0.99$. Taking a magnon Fock space size to 12 in order to implement this thermal state in the simulations, we find an average gate fidelity $\bar{F} = 99.36\%$.

We note that by flux-driving both qubits, a concept we introduce in the next section, we can effectively turn-off the gate when required. In this case, the coupling constant g_Z is proportional to $1/(\omega_m - \omega_{ac})$, where ω_{ac} is the driving frequency. Flux-driving at frequencies much

larger than the magnon frequency can therefore be used to increase the detuning $\omega_m - \omega_{ac}$ such that the coupling is negligible, allowing to realize the gate efficiently by turning off the coupling in this manner after the gate time [79].

C. iCNOT

We consider the limit $a_{J_1} \rightarrow 0$ for one qubit, let it be qubit 1. For qubit 2 we set $a_{J_2} \rightarrow 1$ and $\varphi_{b_2} = \pi/2$. This gives $J_1, g_2 \rightarrow 0$. In order to make the interaction term leading to the iCNOT gate energetically allowed, in this case we need to consider a weak external ac bias $\Phi_b = \Phi_{ac} \cos(\omega_{act})$ with amplitude Φ_{ac} and frequency ω_{ac} applied to the first qubit. This changes the flux $\varphi_b \rightarrow \varphi_{ac} \cos(\omega_{act})$, where $\varphi_{ac} = \pi\Phi_{ac}/\Phi_0$. For $\varphi_{ac} \ll 1$ we find $g(\varphi_b) \rightarrow \tilde{g} \cos(\omega_{act})$, with [41]

$$\tilde{g} = -\frac{\mu_0 I_x \mu_{zpf} e^r}{8\Phi_0 d} \sqrt{8E_C E_J^2} \varphi_{ac}. \quad (33)$$

In the rotating frame of the drive we obtain

$$\begin{aligned} \hat{H}_{\text{RF}}^{\text{iCNOT}} &= \hbar \delta_m \hat{m}^\dagger \hat{m} + \sum_{i=1,2} \hbar \delta_{q_i} \hat{c}_i^\dagger \hat{c}_i + \frac{\hbar \tilde{g}_1}{2} \hat{c}_1^\dagger \hat{c}_1 (\hat{m}^\dagger + \hat{m}) \\ &+ \hbar J_2 (\hat{c}_2^\dagger \hat{m} + \hat{c}_2 \hat{m}^\dagger), \end{aligned} \quad (34)$$

where we defined $\delta_m = \omega_m - \omega_{ac}$ and $\delta_{q_i} = \omega_{q_i} - \omega_{ac}$ and used the rotating wave approximation, which is valid for $\tilde{g}_1 \ll 4\omega_{ac}$. Performing a SW as detailed in Appendix C 3 and choosing $\omega_{ac} = \omega_{q_2} + J_2^2/(\omega_{q_2} - \omega_m)$ yields

$$\begin{aligned} \hat{H}_{\text{SW}}^{\text{iCNOT}} &= \hbar \left(\delta_m - \frac{J_2^2}{\delta_{q_2} - \delta_m} \right) \hat{m}^\dagger \hat{m} \\ &+ \hbar \left(\delta_{q_1} - \frac{\tilde{g}_1^2}{4\delta_m} \right) \hat{\sigma}_1^z + \hbar \tilde{g}_{\text{NOT}} \hat{\sigma}_1^z (\hat{\sigma}_2^+ + \hat{\sigma}_2^-) \end{aligned} \quad (35)$$

with the coupling strength

$$\tilde{g}_{\text{NOT}} = \frac{\tilde{g}_1 J_2}{4} \left(\frac{1}{\delta_{q_2} - \delta_m} - \frac{1}{\delta_m} \right). \quad (36)$$

The frequency of the flux drive ω_{ac} is chosen by matching the Stark-shifted frequency of the second qubit in order to make the interaction term resonant. The SW transformation is valid for $J_2 \ll \omega_{q_2} - \omega_m$ and $\tilde{g}_1 \ll 2\delta_m$. Time propagation of the coupling term of the effective Hamiltonian of Eq. (39) up to $T_{\text{NOT}} = \pi/(2|\tilde{g}_{\text{NOT}}|)$ gives an iCNOT gate

$$\hat{U}_{\text{iCNOT}} = |0\rangle\langle 0| \otimes \hat{I} \mp i |1\rangle\langle 1| \otimes \hat{\sigma}_x, \quad (37)$$

since $\exp(-i\tilde{g}_{\text{NOT}} T_{\text{NOT}} \hat{\sigma}_1^z (\hat{\sigma}_2^+ + \hat{\sigma}_2^-)) = \hat{U}_{\text{iCNOT}}$. This gate resembles a CNOT gate, but adds a phase $\mp i$ if the control qubit, i.e. the first qubit, is excited. Thus, we denominate it an iCNOT gate. The sign of the phase $\mp i$ corresponds to $\tilde{g}_{\text{NOT}} \gtrless 0$.

Similarly as performed for the previous gates, in order to compensate for single qubit rotations we cancel the diagonal term of the control qubit of Eq. (35) by performing the unitary rotation

$$\hat{U}_{\text{SQ}}(t) = \exp \left[it \left(\delta_{q_1} - \frac{\tilde{g}_1^2}{4\delta_m} \right) \hat{\sigma}_1^z \right]. \quad (38)$$

For Eqs. 35 and (34) we find, respectively,

$$\hat{H}_{\text{eff}}^{\text{iCNOT}} = \hbar \left(\delta_m - \frac{J_2^2}{\delta_{q_2} - \delta_m} \right) \hat{m}^\dagger \hat{m} + \hbar \tilde{g}_{\text{NOT}} \hat{\sigma}_1^z (\hat{\sigma}_2^+ + \hat{\sigma}_2^-). \quad (39)$$

Rotating the Hamiltonian before the SW transformation of Eq. (34) with the same unitary transformation yields

$$\begin{aligned} \hat{H}_{\text{tot}}^{\text{iCNOT}} &= \hbar \delta_m \hat{m}^\dagger \hat{m} + \frac{\hbar \tilde{g}_1^2}{4\delta_m} \hat{c}_1^\dagger \hat{c}_1 + \hbar \delta_{q_2} \hat{c}_2^\dagger \hat{c}_2 \\ &+ \frac{\hbar \tilde{g}_1}{2} \hat{c}_1^\dagger \hat{c}_1 (\hat{m}^\dagger + \hat{m}) + \hbar J_2 (\hat{c}_2^\dagger \hat{m} + \hat{c}_2 \hat{m}^\dagger). \end{aligned} \quad (40)$$

For the channel $\mathcal{E}_{\text{iCNOT}}[\rho]$ we use the total Hamiltonian of Eq. (40). We compute the average fidelity of the proposed gate $\mathcal{E}_{\text{iCNOT}}(\rho)$ with the ideal gate \hat{U}_{iCNOT} , which can be found in Eq (37). The result is shown in Fig. 5(a). The dependence of the average gate fidelity on the magnon frequency is akin to the iSWAP gate. The coupling constant \tilde{g}_{NOT} reminds us of a combination of g_S and g_Z of Eqs. (22) and (28), respectively. Since $\delta_{q_2} - \delta_m = \omega_{q_2} - \omega_m$, magnon frequencies close to the frequency of the target qubit give rise to large coupling strengths, but approach the breakdown of the SW transformation, as signalled by a vanishing gate time in Fig. 5(a). Also, the factor δ_m is small for these magnon frequencies due to $\omega_{ac} \approx \omega_{q_2}$. Similarly to the iSWAP gate, magnon frequencies in this regime lead to little increase of the coupling constant due to squeezing: $\tilde{g}_{\text{NOT}} \propto e^{2r} \approx 1$. In order to increase the coupling constant through squeezing one needs $\omega_m \ll \gamma\mu_0 M_s$. Thus, the competition to maximize the coupling constant and hence to restrict dissipative processes is similar to the iSWAP gate.

For the results displayed in Fig. 5 we set the asymmetry parameter and reduced flux of the first (second) qubit to $a_{J_1} = 0$ and $\varphi_{ac_1} = \pi/10$ ($a_{J_2} = 0.9$ and $\varphi_{b_2} = \pi/2$), corresponding to $\omega_{q_1} = 6.2$ GHz ($\omega_{q_2} = 6.0$ GHz). We find a maximum average fidelity of $\bar{F} = 88.66\%$ for $\omega_m/\omega_{q_2} = 0.97$, at an effective coupling strength of $\tilde{g}_{\text{NOT}}/\omega_{q_2} = 7.6 \times 10^{-6}$ corresponding to $\tilde{g}_{\text{NOT}}/(2\pi) = 46$ kHz.

Fig. 5(b) displays the dynamics of the system for the magnon frequency which maximizes the average fidelity and $|10\rangle$ as our input state. At $t = T_{\text{NOT}}$ we should find the state $\hat{U}_{\text{iCNOT}} |10\rangle = -i|11\rangle$. However, due to a relatively large gate time $T_{\text{NOT}} = 5.5 \mu\text{s}$ compared to decay T_1 and dephasing T_ϕ , dissipation has a relatively large influence. Therefore, we see that the control qubit, i.e. the first qubit, has lost some of its initial excitation. The

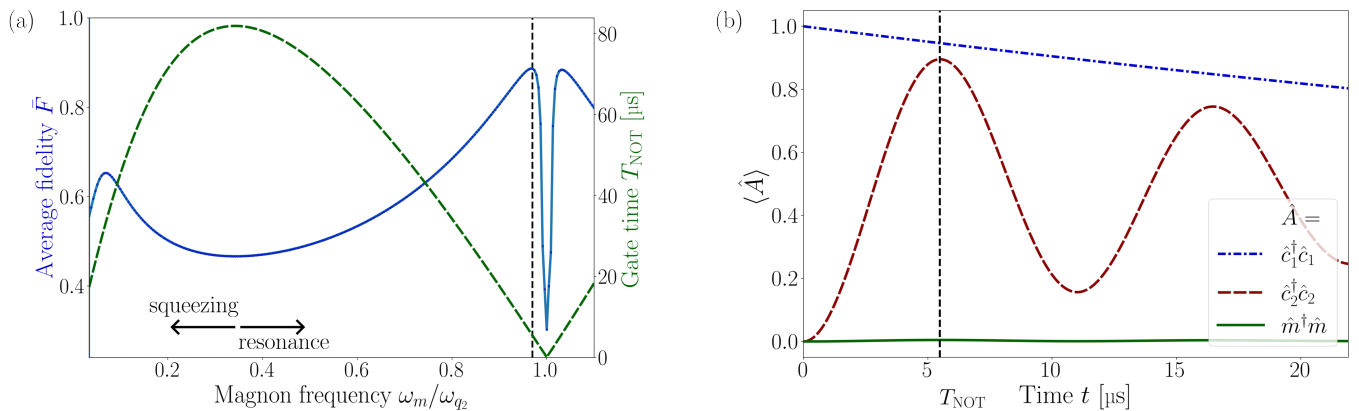


FIG. 5: (a) Average fidelity \bar{F} (blue, solid) and gate time T_{NOT} (green, dashed) of the iCNOT gate as a function of the magnon frequency ω_m . The competition of magnon squeezing versus magnon-qubit resonance to optimize the gate fidelity is similar to the iSWAP gate of Fig. 3. The maximum fidelity, $\bar{F} = 88.66\%$, is found at $\omega_m/\omega_{q_2} = 0.97$ (vertical dashed line). (b) Qubit and magnon dynamics following the evolution with the Hamiltonian of Eq. (40) including dissipation. We use the magnon frequency $\omega_m = 0.97\omega_{q_2}$ found in (a). The occupations of both qubits (blue, dash-dotted and red, dashed) and magnons (green, solid) as a function of time are shown. The target state is $\hat{U}_{\text{iCNOT}}|10\rangle = -i|11\rangle$ at the gate time $T_{\text{NOT}} = 5.5 \mu\text{s}$ (vertical dashed line). Parameters are as in Fig 3.

target qubit does not reach $\langle \hat{c}_2^\dagger \hat{c}_2 \rangle = 1$ either. Turning off the coupling after the gate time T_{NOT} can be simply achieved by switching off the ac driving of the control qubit.

Although the iSWAP and iCNOT gate have some resemblances regarding the effective coupling strength \tilde{g}_{NOT} , the iCNOT gate does not achieve a similar fidelity. The reason is that \tilde{g}_{NOT} is proportional to \tilde{g}_1 , which is a factor 10 smaller than its iSWAP equivalent J_1 , leading to a more detrimental effect of dissipation.

IV. CONCLUSIONS

We have theoretically demonstrated that magnons can be used to mediate strong qubit-qubit coupling, where for feasible experimental parameters we obtained coupling strengths surpassing the qubit dissipation. The coherent magnon-qubit exchange interaction and radiation-pressure interaction can be adopted to engineer two-qubit quantum gates. With the exchange interaction an iSWAP gate is realized by using highly asymmetric SQUIDS. The non-linear interaction generated by symmetric SQUIDS realizes a CZ gate. By combining the exchange interaction on a highly asymmetric SQUID and the radiation-pressure on a symmetric SQUID an iCNOT gate is implemented. We numerically tested these proposed gates under realistic experimental conditions and find an average gate fidelity which equals 99.00% for the iSWAP gate, 99.43% for the CZ gate and 88.66% for the iCNOT gate. The coupling strengths with respect to the qubit dissipation equal $T_{1GS}/(2\pi) = 49$ for the iSWAP, $T_{1GZ}/(2\pi) = 214$ for the CZ and $T_1\tilde{g}_{\text{NOT}}/(2\pi) = 4.6$ for the iCNOT gate. Furthermore, we found no leakage out of the computational space for both qubits.

In all of our simulations, we assumed the initial magnonic state to be vacuum instead of a thermal state for computational simplicity. We found that the optimal magnon frequency for the iSWAP and iCNOT gate is in the gigahertz regime, and thus vacuum state assumption can be achieved passively by cooling the system down to temperatures < 50 mK. However, the optimal magnon frequencies we found for the CZ gate is in the megahertz regime, leading to a sizeable thermal population of magnons for the temperature used in the simulations (10 mK). In order to verify the validity of our results, we simulated the CZ gate further with an initial magnon thermal state dictated by the optimal magnon frequency at the given temperature, and found a similar average fidelity $\bar{F} = 99.36\%$.

While the average gate fidelities for the iSWAP and CZ gates are above the error correction threshold [10, 11], this is not the case for the iCNOT, for which the gate time is not small with respect to the qubit relaxation timescales. One could improve this by introducing waveguides that transport the electromagnetic wave emitted by the magnet to the SQUID loop [56], thereby increasing the total flux through the loop and, as a result, the coupling. Moreover, we have shown that the qubit-magnon coupling strength can be enhanced with magnetization squeezing for magnon frequencies much lower than $\gamma\mu_0 M_s$, and using qubit frequencies close to this regime. However, transmons typically operate at higher frequencies in the 4-8 GHz regime [78]. Therefore, the performance of the iSWAP and iCNOT gates could be further improved in qubit-magnon hybrid systems involving low-frequency qubits [80, 81]. For lower operating frequencies the impact of thermal occupation should be evaluated.

ACKNOWLEDGMENTS

S.S., M.K., and S.V.K. acknowledge financial support by the German Federal Ministry of Education

and Research (BMBF) project QECHQS (Grant No. 16KIS1590K). S.V.K. and Y.M.B. acknowledge financial support by the EU-Project No. HORIZON-EIC-2021-PATHFINDEROPEN-01 PALANTIRI-101046630.

Appendix A: Geometrical factor

With the scalar potential $P(\mathbf{r})$ caused by the magnetization and which obeys $\mathbf{B} = -\mu_0 \nabla P(\mathbf{r})$, we describe the magnetic stray field \mathbf{B} . We decompose the potential in terms which are given rise to by the magnetic moment of each Cartesian component, such that

$$P(\mathbf{r}) = \sum_{i=x,y,z} \mu_i p_i(\mathbf{r}). \quad (\text{A1})$$

We use the magnetic field which is caused by μ_z to obtain Fig. 6, where we plotted the z component of this field and used $\mu_z = M_s V_m$. We set the magnetic moment of the x and y component equal to the magnetic moment fluctuations of Eq. (6) and treat them as operators, so $\mu_x = \Delta \hat{\mu}_x$ and $\mu_y = \Delta \hat{\mu}_y$. We determine the flux through the SQUID loop caused by these fluctuations with

$$\Phi(\Delta \hat{\mu}) = -\mu_0 \sum_{i=x,y} \Delta \hat{\mu}_i \int_{\text{SQUID}} \nabla p_i(\mathbf{r}) \cdot d\mathbf{A}. \quad (\text{A2})$$

By comparing this relation with Eq. (8), we find

$$I_i = -4\pi \int_{\text{SQUID}} \nabla p_i(\mathbf{r}) \cdot d\mathbf{A}. \quad (\text{A3})$$

Due to the symmetry of the setup we find $I_y = 0$.

As described in the main text, a limiting factor of I_x is the superconducting critical field B_c . The amplitude of the stray magnetic field in the z direction, B_z , at $z = d$ should be smaller than B_c . For the magnet with an ellipsoidal shape, the field $B_z(z = L_z)$ is about two orders of magnitude lower than the critical field of typical superconductors [66], as one can see in Fig. 6. Thus, the SQUID loop can be positioned at touching distance from the magnet and hence we set $d - L_z = 10$ nm. Furthermore, L_x and L_z should be chosen such that $N_T \approx 1/2$. However, $L_x \gg L_z$ resembles a magnet infinitely stretched along x axis, which is known to have less magnetic field in its direct vicinity in the $x = 0$ plane than a spherical magnet. Therefore, we set $N_T = 0.45$, which fixes the ratio of L_x and L_z . Increasing the loop radius R leads to an increase in the coupling strength, yet gives rise to more qubit noise. We put $R = 25$ μm . By varying L_x we find an optimal effective coupling constant for $L_x = 16$ μm and $L_z = 3.9$ μm . This corresponds to $I_x = -0.12/\mu\text{m}$. Note that coherent magnon quantum states have been demonstrated in magnets of sizes up to 1 mm [40], significantly larger than the sizes considered here.

Considering a sphere with the same volume and with radius \tilde{r} such that $\tilde{r}^3 = L_x L_z^2$, while fixing $d - \tilde{r} = 10$ nm, gives an effective coupling constant which is a factor 2.8 higher than the coupling constant for an ellipsoidal magnet excluding the squeezing enhancement.

Appendix B: Average gate fidelity

To determine the average gate fidelity efficiently we use the following relation [71],

$$\bar{F}(\mathcal{E}, \hat{U}) = \frac{\sum_j \text{tr} [\hat{U}_j^\dagger \hat{U}^\dagger \mathcal{E}[\hat{U}_j] \hat{U}] + d^2}{d^2(d+1)}, \quad (\text{B1})$$

where the unitary operators \hat{U}_j form an orthogonal basis and $d = 4$ is the dimension of the two-qubit space. We choose $\hat{U}_j = \hat{\sigma}_k \otimes \hat{\sigma}_l$, where $\hat{\sigma}_m$ is identity or a Pauli matrix, so $\hat{\sigma}_m \in \{\hat{I}, \hat{\sigma}_x, \hat{\sigma}_y, \hat{\sigma}_z\}$. The input of $\mathcal{E}[\hat{\rho}]$ is restricted to density matrices. Since the Pauli matrices have zero trace, we write these in terms of the density matrices. We find $\hat{I} = \hat{\rho}_0 + \hat{\rho}_1$, $\hat{\sigma}_x = 2\hat{\rho}_+ - \hat{\rho}_0 - \hat{\rho}_1$, $\hat{\sigma}_y = 2\hat{\rho}_{i-} - \hat{\rho}_0 - \hat{\rho}_1$ and $\hat{\sigma}_z = \hat{\rho}_0 - \hat{\rho}_1$. Here, $\hat{\rho}_i = |i\rangle\langle i|$, $|+\rangle = \frac{1}{\sqrt{2}}(|0\rangle + |1\rangle)$ and $|i-\rangle = \frac{1}{\sqrt{2}}(|0\rangle - i|1\rangle)$. We use the linearity of $\mathcal{E}[\hat{\rho}]$ to rewrite the expressions. For example, one finds

$$\mathcal{E}[\hat{I} \otimes \hat{\sigma}_x] = 2\mathcal{E}[\hat{\rho}_0 \otimes \hat{\rho}_+] - \mathcal{E}[(\hat{\rho}_0 \otimes \hat{\rho}_0) - \mathcal{E}[\hat{\rho}_0 \otimes \hat{\rho}_1] + 2\mathcal{E}[\hat{\rho}_1 \otimes \hat{\rho}_+] - \mathcal{E}[\hat{\rho}_1 \otimes \hat{\rho}_0] - \mathcal{E}[\hat{\rho}_1 \otimes \hat{\rho}_1]. \quad (\text{B2})$$

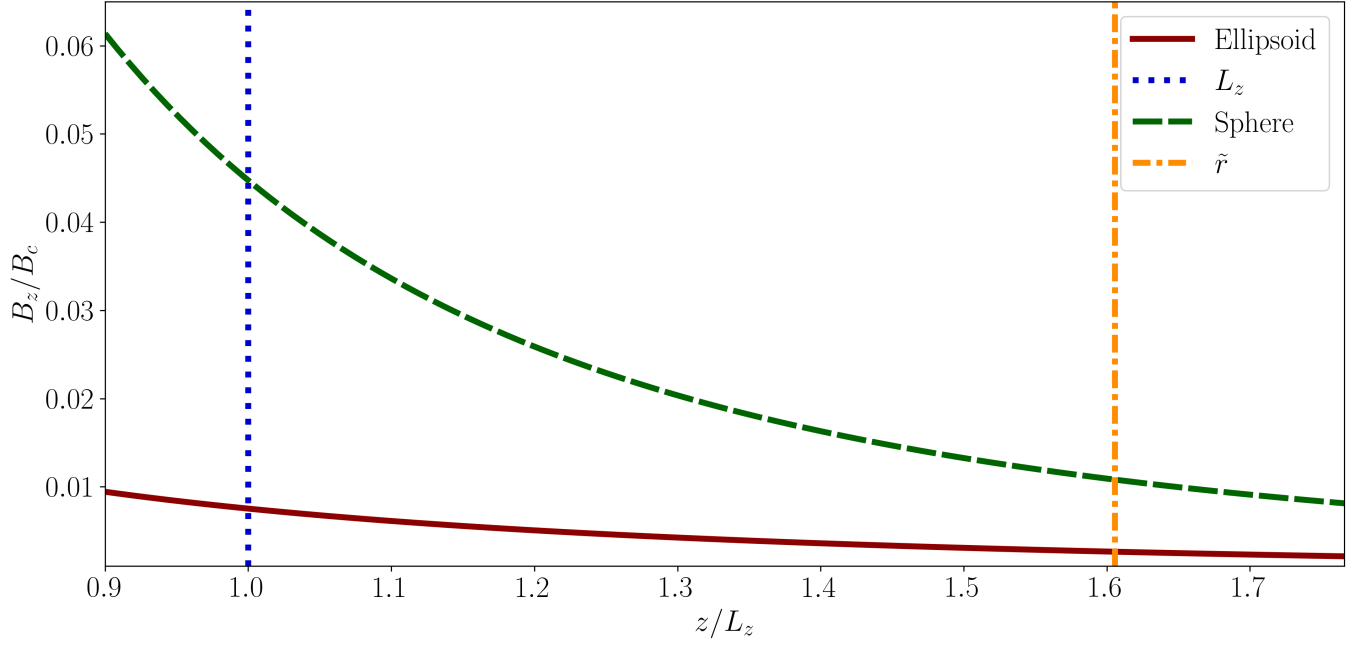


FIG. 6: Magnetic field in z direction in units of the critical field B_c for an ellipsoidal and spherical magnet as a function of the distance z in units of L_z .

Appendix C: Schrieffer-Wolff transformation

With a SW transformation one transforms a Hamiltonian \hat{H} according to $\hat{H}_{\text{SW}} = e^{-\hat{S}} \hat{H} e^{\hat{S}}$ with an anti-Hermitian generator $\hat{S} = -\hat{S}^\dagger$. We write $\hat{H} = \hat{H}_0 + \hat{H}_{\text{int}}$, where \hat{H}_0 is already diagonalized with respect to the tensor product of the number basis for qubits and magnon, on the contrary to \hat{H}_{int} . We assume that both \hat{S} and \hat{H}_{int} are proportional to a coupling constant (e.g. J or g). We approximate to second order in this constant. Using the Baker-Campbell-Hausdorff formula to second order gives

$$\hat{H}_{\text{SW}} \approx \hat{H}_0 + \hat{H}_{\text{int}} + [\hat{S}, \hat{H}_0] + [\hat{S}, \hat{H}_{\text{int}}] + \frac{1}{2} [\hat{S}, [\hat{S}, \hat{H}_0]].$$

By imposing $[\hat{S}, \hat{H}_0] = -\hat{H}_{\text{int}}$ one gets

$$\hat{H}_{\text{SW}} = \hat{H}_0 + \frac{1}{2} [\hat{S}, \hat{H}_{\text{int}}].$$

This approximation is valid for $|\hat{S}| \ll 1$.

The diagonalized Hamiltonian can be found in Eq. (13) and the interaction Hamiltonian in Eq. (15). We use the generator $\hat{S} = \hat{S}_J + \hat{S}_g$, where

$$\hat{S}_J = \sum_{i=1,2} J_i (\chi_i (\hat{c}_i^\dagger \hat{c}_i) \hat{c}_i^\dagger \hat{m} - \hat{c}_i \hat{m}^\dagger \chi_i (\hat{c}_i^\dagger \hat{c}_i)), \quad (\text{C1})$$

with transmon susceptibility

$$\chi_i (\hat{c}_i^\dagger \hat{c}_i) = \frac{1}{\omega_m - \omega_{q_i} + \frac{E_C}{\hbar} (\hat{c}_i^\dagger \hat{c}_i - 1)}, \quad (\text{C2})$$

and

$$\hat{S}_g = \sum_{i=1,2} \frac{g_i}{\omega_m} \hat{c}_i^\dagger \hat{c}_i (\hat{m}^\dagger - \hat{m}). \quad (\text{C3})$$

We compute

$$\begin{aligned}
[\hat{S}_J, \hat{H}_0] &= \sum_{i=1,2} \left[J_i (\chi_i (\hat{c}_i^\dagger \hat{c}_i) \hat{c}_i^\dagger \hat{m} - \hat{c}_i \hat{m}^\dagger \chi_i (\hat{c}_i^\dagger \hat{c}_i)), \hbar \omega_q \hat{c}_i^\dagger \hat{c}_i - \frac{E_C}{2} \hat{c}_i^\dagger \hat{c}_i^\dagger \hat{c}_i \hat{c}_i \right] \\
&\quad + \sum_{i=1,2} \left[J_i (\chi_i (\hat{c}_i^\dagger \hat{c}_i) \hat{c}_i^\dagger \hat{m} - \hat{c}_i \hat{m}^\dagger \chi_i (\hat{c}_i^\dagger \hat{c}_i)), \hbar \omega_m \hat{m}^\dagger \hat{m} \right] \\
&= - \sum_{i=1,2} \hbar J_i (\hat{c}_i \hat{m}^\dagger + \hat{c}_i^\dagger \hat{m}) = - \sum_{i=1,2} \hat{H}_J^i
\end{aligned} \tag{C4}$$

and

$$[\hat{S}_g, \hat{H}_0] = \sum_{i=1,2} \hbar g_i \hat{c}_i^\dagger \hat{c}_i [\hat{m}^\dagger - \hat{m}, \hat{m}^\dagger \hat{m}] = - \sum_{i=1,2} \hbar g_i \hat{c}_i^\dagger \hat{c}_i (\hat{m}^\dagger + \hat{m}) = - \sum_{i=1,2} \hat{H}_g^i. \tag{C5}$$

Thus, we verify

$$[\hat{S}, \hat{H}_0] = [\hat{S}_J, \hat{H}_0] + [\hat{S}_g, \hat{H}_0] = - \sum_{i=1,2} \hat{H}_J^i + \hat{H}_g^i = - \hat{H}_{\text{int}}. \tag{C6}$$

This leaves us to determine

$$[\hat{S}, \hat{H}_{\text{int}}] = \hat{H}_{J,J} + \hat{H}_{J,g} + \hat{H}_{g,J} + \hat{H}_{g,g}, \tag{C7}$$

with $\hat{H}_{J,J} = [\hat{S}_J, \sum_{i=1,2} \hat{H}_J^i]$, $\hat{H}_{J,g} = [\hat{S}_J, \sum_{i=1,2} \hat{H}_g^i]$, $\hat{H}_{g,J} = [\hat{S}_g, \sum_{i=1,2} \hat{H}_J^i]$ and $\hat{H}_{g,g} = [\hat{S}_g, \sum_{i=1,2} \hat{H}_g^i]$. We find

$$\begin{aligned}
\hat{H}_{J,J} &= \sum_{i=1,2} \hbar J_i^2 \left(2\chi_i (\hat{c}_i^\dagger \hat{c}_i) \hat{c}_i^\dagger \hat{c}_i - (2\chi_i (\hat{c}_i^\dagger \hat{c}_i + 1)(1 - \hat{c}_i^\dagger \hat{c}_i) + 2\chi_i (\hat{c}_i^\dagger \hat{c}_i) \hat{c}_i^\dagger \hat{c}_i) \hat{m}^\dagger \hat{m} \right. \\
&\quad \left. + (\chi_i (\hat{c}_i^\dagger \hat{c}_i) - \chi_i (\hat{c}_i^\dagger \hat{c}_i - 1)) (\hat{c}_i^\dagger)^2 \hat{m}^2 + (\chi_i (\hat{c}_i^\dagger \hat{c}_i + 2) - \chi_i (\hat{c}_i^\dagger \hat{c}_i + 1)) \hat{c}_i^2 (\hat{m}^\dagger)^2 \right) \\
&\quad + \hbar J_1 J_2 \left(\chi_1 (\hat{c}_1^\dagger \hat{c}_1) \hat{c}_1^\dagger \hat{c}_2 + \hat{c}_1 \chi_1 (\hat{c}_1^\dagger \hat{c}_1) \hat{c}_2^\dagger \right) + \hbar J_1 J_2 \left(\chi_2 (\hat{c}_2^\dagger \hat{c}_2) \hat{c}_2^\dagger \hat{c}_1 + \hat{c}_2 \chi_2 (\hat{c}_2^\dagger \hat{c}_2) \hat{c}_1^\dagger \right),
\end{aligned} \tag{C8}$$

$$\begin{aligned}
\hat{H}_{J,g} &= \sum_{i=1,2} \hbar J_i g_i \left(\chi_i (\hat{c}_i^\dagger \hat{c}_i) \hat{c}_i^\dagger (\hat{c}_i^\dagger \hat{c}_i - (\hat{m} + \hat{m}^\dagger) \hat{m}) + \chi_i (\hat{c}_i^\dagger \hat{c}_i + 1) \hat{c}_i (\hat{c}_i^\dagger \hat{c}_i - (\hat{m} + \hat{m}^\dagger) \hat{m}^\dagger) \right) \\
&\quad + \hbar J_1 g_2 \hat{c}_2^\dagger \hat{c}_2 \left(\chi_1 (\hat{c}_1^\dagger \hat{c}_1) \hat{c}_1^\dagger + \hat{c}_1 \chi_1 (\hat{c}_1^\dagger \hat{c}_1) \right) + \hbar g_1 J_2 \hat{c}_1^\dagger \hat{c}_1 \left(\chi_2 (\hat{c}_2^\dagger \hat{c}_2) \hat{c}_2^\dagger + \hat{c}_2 \chi_2 (\hat{c}_2^\dagger \hat{c}_2) \right),
\end{aligned} \tag{C9}$$

$$\begin{aligned}
\hat{H}_{g,J} &= \sum_{i=1,2} \frac{\hbar J_i g_i}{\omega_m} \left((\hat{c}_i^\dagger + \hat{c}_i) (\hat{m}^\dagger \hat{m} + 1) - \hat{c}_i (\hat{m}^\dagger)^2 - \hat{c}_i^\dagger \hat{m}^2 - \hat{c}_i^\dagger \hat{c}_i \hat{c}_i^\dagger - \hat{c}_i \hat{c}_i^\dagger \hat{c}_i \right) \\
&\quad - \frac{\hbar g_1 J_2}{\omega_m} \hat{c}_1^\dagger \hat{c}_1 (\hat{c}_2^\dagger + \hat{c}_2) - \frac{\hbar J_1 g_2}{\omega_m} (\hat{c}_1^\dagger + \hat{c}_1) \hat{c}_2^\dagger \hat{c}_2
\end{aligned} \tag{C10}$$

and finally

$$\hat{H}_{g,g} = - \sum_{i=1,2} \frac{2\hbar g_i^2}{\omega_m} (\hat{c}_i^\dagger \hat{c}_i)^2 - \frac{4\hbar g_1 g_2}{\omega_m} \hat{c}_1^\dagger \hat{c}_1 \hat{c}_2^\dagger \hat{c}_2. \tag{C11}$$

Thus, the transformed Hamiltonian we obtain is

$$\hat{H}_{\text{SW}} = \hat{H}_0 + \frac{1}{2} \left(\hat{H}_{J,J} + \hat{H}_{J,g} + \hat{H}_{g,J} + \hat{H}_{g,g} \right). \tag{C12}$$

We note that Eq. (C8) contains a SWAP-like qubit-qubit term, Eqs. (C9) and (C10) show a controlled-SWAP form and Eq. (C11) a controlled-phase term. By choosing different combinations of coupling constants J and g , we can tune between these interactions.

1. iSWAP

For $g_1 = g_2 = 0$ we find $\hat{H}_{J,g} = \hat{H}_{g,J} = \hat{H}_{g,g} = 0$. Therefore, we find

$$\hat{H}_{\text{SW}}^{\text{iSWAP}} = \hat{H}_0 + \frac{1}{2}\hat{H}_{J,J}. \quad (\text{C13})$$

Truncating the qubit levels such that the ground state and first excited state remains gives

$$\hat{H}_{J,J} = \sum_{i=1,2} 2\hbar J_i^2 \chi_i(1)(\hat{\sigma}_i^z - \hat{m}^\dagger \hat{m}) + \hbar J_1 J_2 (\chi_1(1) + \chi_2(1))(\hat{\sigma}_1^+ \hat{\sigma}_2^- + \hat{\sigma}_1^- \hat{\sigma}_2^+). \quad (\text{C14})$$

This leads to Eq. (21).

2. CZ

For $J_1 = J_2 = 0$ we have $\hat{H}_{J,J} = \hat{H}_{J,g} = \hat{H}_{g,J} = 0$. This gives

$$\hat{H}_{\text{SW}}^{\text{iSWAP}} = \hat{H}_0 + \frac{1}{2}\hat{H}_{g,g}. \quad (\text{C15})$$

Taking only the ground and first state of the qubit gives

$$\hat{H}_{g,g} = - \sum_{i=1,2} \frac{2\hbar g_i^2}{\omega_m} \sigma_i^z - \frac{4\hbar g_1 g_2}{\omega_m} \hat{\sigma}_1^z \hat{\sigma}_2^z, \quad (\text{C16})$$

since for qubits $(\hat{c}_i^\dagger \hat{c}_i)^2 = \hat{c}_i^\dagger \hat{c}_i$. This yields Eq. (27).

3. iCNOT

We set $J_1 = g_2 = 0$. Since $\hat{H}_{J,J}$, $\hat{H}_{J,g}$, $\hat{H}_{g,J}$ and $\hat{H}_{g,g}$ do not vanish, the transformed Hamiltonian is given by Eq. (C12). From now on, we limit the qubit to its lowest two levels. Eq. (34) shows that we can use the results of the SW transformation if we implement following substitutions: $\omega_m \rightarrow \delta_m$, $\omega_{q_i} \rightarrow \delta_{q_i}$ and $g_1 \rightarrow \tilde{g}_1/2$. We find

$$\hat{H}_{J,J} = \frac{2\hbar J_2^2}{\delta_m - \delta_{q_i}} (\hat{\sigma}_2^z - \hat{m}^\dagger \hat{m}), \quad (\text{C17})$$

$$\hat{H}_{J,g} = \frac{\hbar \tilde{g}_1 J_2}{2(\delta_{q_2} - \delta_m)} \hat{\sigma}_1^z (\hat{\sigma}_2^+ + \hat{\sigma}_2^-), \quad (\text{C18})$$

$$\hat{H}_{g,J} = -\frac{\hbar \tilde{g}_1 J_2}{2\delta_m} \hat{\sigma}_1^z (\hat{\sigma}_2^+ + \hat{\sigma}_2^-) \quad (\text{C19})$$

and

$$\hat{H}_{g,g} = -\frac{\hbar \tilde{g}_1^2}{2\delta_m} \hat{\sigma}_1^z. \quad (\text{C20})$$

With Eq. (C12) we find

$$\begin{aligned} \hat{H}_{\text{SW}}^{\text{iCNOT}} = & \hbar \left(\delta_m - \frac{J_2^2}{\delta_{q_2} - \delta_m} \right) \hat{m}^\dagger \hat{m} + \hbar \left(\delta_{q_1} - \frac{\tilde{g}_1^2}{4\delta_m} \right) \hat{\sigma}_1^z + \hbar \left(\delta_{q_2} + \frac{J_2^2}{\delta_{q_2} - \delta_m} \right) \hat{\sigma}_2^z \\ & + \frac{\hbar \tilde{g}_1 J_2}{4} \left(\frac{1}{\delta_{q_2} - \delta_m} - \frac{1}{\delta_m} \right) \hat{\sigma}_1^z (\hat{\sigma}_2^+ + \hat{\sigma}_2^-). \end{aligned} \quad (\text{C21})$$

We cancel the frequency of the target qubit by setting $\omega_{\text{ac}} = \omega_{q_2} + J_2^2/(\omega_{q_2} - \omega_m)$. This gives Eq. (35).

[1] G. Kurizki, P. Bertet, Y. Kubo, K. Mølmer, D. Petrosyan, P. Rabl, and J. Schmiedmayer, Quantum tech-

nologies with hybrid systems, Proceedings of the National

- Academy of Sciences **112**, 3866 (2015).
- [2] A. Clerk, K. Lehnert, P. Bertet, J. Petta, and Y. Nakamura, Hybrid quantum systems with circuit quantum electrodynamics, *Nature Physics* **16**, 10.1038/s41567-020-0797-9 (2020).
 - [3] D. Vion, A. Aassime, A. Cottet, P. Joyez, H. Pothier, C. Urbina, D. Esteve, and M. H. Devoret, Manipulating the quantum state of an electrical circuit, *Science* **296**, 886 (2002).
 - [4] J. Clarke and F. Wilhelm, Superconducting quantum bits, *Nature* **453**, 1031 (2008).
 - [5] F. Arute, K. Arya, R. Babbush, J. Bardin, R. Barends, R. Biswas, S. Boixo, F. Brandao, D. Buell, B. Burkett, Y. Chen, Z. Chen, B. Chiaro, R. Collins, W. Courtney, A. Dunsworth, E. Farhi, B. Foxen, and J. Martinis, Quantum supremacy using a programmable superconducting processor, *Nature* **574**, 505 (2019).
 - [6] J. M. Chow, L. DiCarlo, J. M. Gambetta, F. Motzoi, L. Frunzio, S. M. Girvin, and R. J. Schoelkopf, Optimized driving of superconducting artificial atoms for improved single-qubit gates, *Phys. Rev. A* **82**, 040305 (2010).
 - [7] R. Barends, J. Kelly, A. Megrant, A. Veitia, D. Sank, E. Jeffrey, T. White, J. Mutus, A. Fowler, B. Campbell, Y. Chen, Z. Chen, B. Chiaro, A. Dunsworth, C. Neill, P. O'Malley, P. Roushan, A. Vainsencher, J. Wenner, and J. Martinis, Superconducting quantum circuits at the surface code threshold for fault tolerance, *Nature* **508**, 500 (2014).
 - [8] D. C. McKay, C. J. Wood, S. Sheldon, J. M. Chow, and J. M. Gambetta, Efficient z gates for quantum computing, *Phys. Rev. A* **96**, 022330 (2017).
 - [9] D. S. Wang, A. G. Fowler, and L. C. L. Hollenberg, Surface code quantum computing with error rates over 1%, *Phys. Rev. A* **83**, 020302 (2011).
 - [10] A. G. Fowler, A. C. Whiteside, and L. C. L. Hollenberg, Towards practical classical processing for the surface code, *Phys. Rev. Lett.* **108**, 180501 (2012).
 - [11] A. G. Fowler, M. Mariantoni, J. M. Martinis, and A. N. Cleland, Surface codes: Towards practical large-scale quantum computation, *Phys. Rev. A* **86**, 032324 (2012).
 - [12] A. Chumak, V. Vasyuchka, A. Serga, and B. Hillebrands, Magnon spintronics, *Nature Physics* **11**, 453–461 (2015).
 - [13] H. Yuan, Y. Cao, A. Kamra, R. A. Duine, and P. Yan, Quantum magnonics: When magnon spintronics meets quantum information science, *Physics Reports* **965**, 1 (2022).
 - [14] B. Zare Rameshti, S. Viola Kusminskiy, J. A. Haigh, K. Usami, D. Lachance-Quirion, Y. Nakamura, C.-M. Hu, H. X. Tang, G. E. Bauer, and Y. M. Blanter, Cavity magnonics, *Physics Reports* **979**, 1 (2022).
 - [15] A. Osada, R. Hisatomi, A. Noguchi, Y. Tabuchi, R. Yamazaki, K. Usami, M. Sadgrove, R. Yalla, M. Nomura, and Y. Nakamura, Cavity optomagnonics with spin-orbit coupled photons, *Phys. Rev. Lett.* **116**, 223601 (2016).
 - [16] T. Liu, X. Zhang, H. X. Tang, and M. E. Flatté, Optomagnonics in magnetic solids, *Phys. Rev. B* **94**, 060405 (2016).
 - [17] S. Viola Kusminskiy, H. X. Tang, and F. Marquardt, Coupled spin-light dynamics in cavity optomagnonics, *Phys. Rev. A* **94**, 033821 (2016).
 - [18] X. Zhang, N. Zhu, C.-L. Zou, and H. X. Tang, Optomagnonic whispering gallery microresonators, *Phys. Rev. Lett.* **117**, 123605 (2016).
 - [19] J. A. Haigh, N. J. Lambert, S. Sharma, Y. M. Blanter, G. E. W. Bauer, and A. J. Ramsay, Selection rules for cavity-enhanced brillouin light scattering from magneto-static modes, *Phys. Rev. B* **97**, 214423 (2018).
 - [20] O. O. Soykal and M. E. Flatté, Strong field interactions between a nanomagnet and a photonic cavity, *Phys. Rev. Lett.* **104**, 077202 (2010).
 - [21] H. Huebl, C. W. Zollitsch, J. Lotze, F. Hocke, M. Greifenstein, A. Marx, R. Gross, and S. T. B. Goennenwein, High cooperativity in coupled microwave resonator ferromagnetic insulator hybrids, *Phys. Rev. Lett.* **111**, 127003 (2013).
 - [22] Y. Tabuchi, S. Ishino, T. Ishikawa, R. Yamazaki, K. Usami, and Y. Nakamura, Hybridizing ferromagnetic magnons and microwave photons in the quantum limit, *Phys. Rev. Lett.* **113**, 083603 (2014).
 - [23] X. Zhang, C.-L. Zou, L. Jiang, and H. X. Tang, Strongly coupled magnons and cavity microwave photons, *Phys. Rev. Lett.* **113**, 156401 (2014).
 - [24] M. Goryachev, W. G. Farr, D. L. Creedon, Y. Fan, M. Kostylev, and M. E. Tobar, High-cooperativity cavity qed with magnons at microwave frequencies, *Phys. Rev. Appl.* **2**, 054002 (2014).
 - [25] M. Weiler, H. Huebl, F. S. Goerg, F. D. Czeschka, R. Gross, and S. T. B. Goennenwein, Spin pumping with coherent elastic waves, *Phys. Rev. Lett.* **108**, 176601 (2012).
 - [26] X. Zhang, C.-L. Zou, L. Jiang, and H. X. Tang, Cavity magnomechanics, *Science Advances* **2**, 10.1126/sciadv.1501286 (2016).
 - [27] K. An, A. N. Litvinenko, R. Kohnno, A. A. Fuad, V. V. Naletov, L. Vila, U. Ebels, G. de Loubens, H. Hurdéquin, N. Beaulieu, J. Ben Youssef, N. Vukadinovic, G. E. W. Bauer, A. N. Slavin, V. S. Tiberkevich, and O. Klein, Coherent long-range transfer of angular momentum between magnon kittel modes by phonons, *Phys. Rev. B* **101**, 060407 (2020).
 - [28] C. A. Potts, E. Varga, V. A. S. V. Bittencourt, S. V. Kusminskiy, and J. P. Davis, Dynamical backaction magnomechanics, *Phys. Rev. X* **11**, 031053 (2021).
 - [29] R. Schlitz, L. Siegl, T. Sato, W. Yu, G. E. W. Bauer, H. Huebl, and S. T. B. Goennenwein, Magnetization dynamics affected by phonon pumping, *Phys. Rev. B* **106**, 014407 (2022).
 - [30] M. Müller, J. Weber, F. Engelhardt, V. A. S. V. Bittencourt, T. Luschmann, M. Cherkasskii, M. Opel, S. T. B. Goennenwein, S. Viola Kusminskiy, S. Geprägs, R. Gross, M. Althammer, and H. Huebl, Chiral phonons and phononic birefringence in ferromagnetic metal–bulk acoustic resonator hybrids, *Phys. Rev. B* **109**, 024430 (2024).
 - [31] F. Casola, T. van der Sar, and A. Yacoby, Probing condensed matter physics with magnetometry based on nitrogen-vacancy centres in diamond, *Nature Reviews Materials* **3**, 10.1038/natrevmats.2017.88 (2018).
 - [32] I. Bertelli, J. J. Carmiggelt, T. Yu, B. G. Simon, C. C. Pothoven, G. E. W. Bauer, Y. M. Blanter, J. Aarts, and T. van der Sar, Magnetic resonance imaging of spin-wave transport and interference in a magnetic insulator, *Science Advances* **6**, eabd3556 (2020).
 - [33] M. Bejarano, F. J. T. Goncalves, T. Hache, M. Hollenbach, C. Heins, T. Hula, L. Körber, J. Heinze, Y. Berencén, M. Helm, J. Fassbender, G. V. Astakhov, and H. Schultheiss, Parametric magnon transduction to spin qubits, *Science Advances* **10**, eadi2042 (2024).

- [34] A. Kamra, W. Belzig, and A. Brataas, Magnon-squeezing as a niche of quantum magnonics, *Applied Physics Letters* **117**, 090501 (2020).
- [35] S. Sharma, V. A. S. V. Bittencourt, A. D. Karenowska, and S. V. Kusminskiy, Spin cat states in ferromagnetic insulators, *Phys. Rev. B* **103**, L100403 (2021).
- [36] V. Cherepanov, I. Kolokolov, and V. L'vov, The saga of yig: Spectra, thermodynamics, interaction and relaxation of magnons in a complex magnet, *Physics Reports* **229**, 81 (1993).
- [37] Y. Tabuchi, S. Ishino, A. Noguchi, T. Ishikawa, R. Yamazaki, K. Usami, and Y. Nakamura, Coherent coupling between a ferromagnetic magnon and a superconducting qubit, *Science* **349**, 405 (2015).
- [38] D. Lachance-Quirion, S. P. Wolski, Y. Tabuchi, S. Kono, K. Usami, and Y. Nakamura, Entanglement-based single-shot detection of a single magnon with a superconducting qubit, *Science* **367**, 425 (2020).
- [39] S. P. Wolski, D. Lachance-Quirion, Y. Tabuchi, S. Kono, A. Noguchi, K. Usami, and Y. Nakamura, Dissipation-based quantum sensing of magnons with a superconducting qubit, *Phys. Rev. Lett.* **125**, 117701 (2020).
- [40] D. Xu, X.-K. Gu, H.-K. Li, Y.-C. Weng, Y.-P. Wang, J. Li, H. Wang, S.-Y. Zhu, and J. Q. You, Quantum control of a single magnon in a macroscopic spin system, *Phys. Rev. Lett.* **130**, 193603 (2023).
- [41] M. Kounalakis, G. E. W. Bauer, and Y. M. Blanter, Analog quantum control of magnonic cat states on a chip by a superconducting qubit, *Phys. Rev. Lett.* **129**, 037205 (2022).
- [42] M. Kounalakis, S. Viola Kusminskiy, and Y. M. Blanter, Engineering entangled coherent states of magnons and phonons via a transmon qubit, *Phys. Rev. B* **108**, 224416 (2023).
- [43] A. Dewes, F. R. Ong, V. Schmitt, R. Lauro, N. Boulant, P. Bertet, D. Vion, and D. Esteve, Characterization of a two-transmon processor with individual single-shot qubit readout, *Phys. Rev. Lett.* **108**, 057002 (2012).
- [44] R. Barends, J. Kelly, A. Megrant, D. Sank, E. Jeffrey, Y. Chen, Y. Yin, B. Chiaro, J. Mutus, C. Neill, P. O'Malley, P. Roushan, J. Wenner, T. C. White, A. N. Cleland, and J. M. Martinis, Coherent josephson qubit suitable for scalable quantum integrated circuits, *Phys. Rev. Lett.* **111**, 080502 (2013).
- [45] A. Kandala, K. X. Wei, S. Srinivasan, E. Magesan, S. Carnevale, G. A. Keefe, D. Klaus, O. Dial, and D. C. McKay, Demonstration of a high-fidelity cnot gate for fixed-frequency transmons with engineered zz suppression, *Phys. Rev. Lett.* **127**, 130501 (2021).
- [46] J. Q. You, Y. Nakamura, and F. Nori, Fast two-bit operations in inductively coupled flux qubits, *Phys. Rev. B* **71**, 024532 (2005).
- [47] M. Grajcar, Y.-x. Liu, F. Nori, and A. M. Zagoskin, Switchable resonant coupling of flux qubits, *Phys. Rev. B* **74**, 172505 (2006).
- [48] A. O. Niskanen, K. Harrabi, F. Yoshihara, Y. Nakamura, S. Lloyd, and J. S. Tsai, Quantum coherent tunable coupling of superconducting qubits, *Science* **316**, 723 (2007).
- [49] Y. Chen, C. Neill, P. Roushan, N. Leung, M. Fang, R. Barends, J. Kelly, B. Campbell, Z. Chen, B. Chiaro, A. Dunsworth, E. Jeffrey, A. Megrant, J. Y. Mutus, P. J. J. O'Malley, C. M. Quintana, D. Sank, A. Vainsencher, J. Wenner, T. C. White, M. R. Geller, A. N. Cleland, and J. M. Martinis, Qubit architecture with high coherence and fast tunable coupling, *Phys. Rev. Lett.* **113**, 220502 (2014).
- [50] M. Kounalakis, C. Dickel, A. Bruno, N. Langford, and G. Steele, Tuneable hopping and nonlinear cross-kerr interactions in a high-coherence superconducting circuit, *npj Quantum Information* **4**, 38 (2018).
- [51] J. Majer, J. M. Chow, J. M. Gambetta, J. Koch, B. R. Johnson, J. A. Schreier, L. Frunzio, D. I. Schuster, A. A. Houck, A. Wallraff, A. Blais, M. H. Devoret, S. M. Girvin, and R. J. Schoelkopf, Coupling superconducting qubits via a cavity bus, *Nature* **449**, 443–447 (2007).
- [52] D. C. McKay, S. Filipp, A. Mezzacapo, E. Magesan, J. M. Chow, and J. M. Gambetta, Universal gate for fixed-frequency qubits via a tunable bus, *Phys. Rev. Appl.* **6**, 064007 (2016).
- [53] M. Roth, M. Ganzhorn, N. Moll, S. Filipp, G. Salis, and S. Schmidt, Analysis of a parametrically driven exchange-type gate and a two-photon excitation gate between superconducting qubits, *Phys. Rev. A* **96**, 062323 (2017).
- [54] Y. Xu, J. Chu, J. Yuan, J. Qiu, Y. Zhou, L. Zhang, X. Tan, Y. Yu, S. Liu, J. Li, F. Yan, and D. Yu, High-fidelity, high-scalability two-qubit gate scheme for superconducting qubits, *Phys. Rev. Lett.* **125**, 240503 (2020).
- [55] J. Chen, T. Yu, C. Liu, T. Liu, M. Madami, K. Shen, J. Zhang, S. Tu, M. S. Alam, K. Xia, M. Wu, G. Gubbiotti, Y. M. Blanter, G. E. W. Bauer, and H. Yu, Excitation of unidirectional exchange spin waves by a nanoscale magnetic grating, *Phys. Rev. B* **100**, 104427 (2019).
- [56] T. Yu, Y.-X. Zhang, S. Sharma, X. Zhang, Y. M. Blanter, and G. E. W. Bauer, Magnon accumulation in chirally coupled magnets, *Phys. Rev. Lett.* **124**, 107202 (2020).
- [57] M. J. Bremner, C. M. Dawson, J. L. Dodd, A. Gilchrist, A. W. Harrow, D. Mortimer, M. A. Nielsen, and T. J. Osborne, Practical scheme for quantum computation with any two-qubit entangling gate, *Physical Review Letters* **89**, 10.1103/physrevlett.89.247902 (2002).
- [58] N. Schuch and J. Siewert, Natural two-qubit gate for quantum computation using the XY interaction, *Phys. Rev. A* **67**, 032301 (2003).
- [59] J. Koch, T. M. Yu, J. Gambetta, A. A. Houck, D. I. Schuster, J. Majer, A. Blais, M. H. Devoret, S. M. Girvin, and R. J. Schoelkopf, Charge-insensitive qubit design derived from the cooper pair box, *Phys. Rev. A* **76**, 042319 (2007).
- [60] D. P. DiVincenzo, The physical implementation of quantum computation, *Fortschritte der Physik* **48**, 771–783 (2000).
- [61] A. Kamra and W. Belzig, Super-poissonian shot noise of squeezed-magnon mediated spin transport, *Phys. Rev. Lett.* **116**, 146601 (2016).
- [62] D. Stancil and A. Prabhakar, *Spin Waves: Theory and Applications* (Springer, New York, 2009).
- [63] J. A. Osborn, Demagnetizing factors of the general ellipsoid, *Phys. Rev.* **67**, 351 (1945).
- [64] C. C. Rusconi, M. J. A. Schuetz, J. Gieseler, M. D. Lukin, and O. Romero-Isart, Hybrid architecture for engineering magnonic quantum networks, *Phys. Rev. A* **100**, 022343 (2019).
- [65] H. Chang, Fields external to open-structure magnetic devices represented by ellipsoid or spheroid, *British Journal of Applied Physics* **12**, 160 (1961).
- [66] M. Popinciuc, V. E. Calado, X. L. Liu, A. R. Akhmerov, T. M. Klapwijk, and L. M. K. Vandersypen, Zero-bias conductance peak and josephson effect in graphene-nbntn

- junctions, *Phys. Rev. B* **85**, 205404 (2012).
- [67] M. Aspelmeyer, T. J. Kippenberg, and F. Marquardt, Cavity optomechanics, *Rev. Mod. Phys.* **86**, 1391 (2014).
- [68] S. Klingler, H. Maier-Flaig, C. Dubs, O. Surzhenko, R. Gross, H. Huebl, S. T. B. Goennenwein, and M. Weiler, Gilbert damping of magnetostatic modes in a yttrium iron garnet sphere, *Applied Physics Letters* **110**, 092409 (2017).
- [69] S. Kosen, A. F. van Loo, D. A. Bozhko, L. Mihalceanu, and A. D. Karenowska, Microwave magnon damping in YIG films at millikelvin temperatures, *APL Materials* **7**, 101120 (2019).
- [70] H. Maier-Flaig, S. Klingler, C. Dubs, O. Surzhenko, R. Gross, M. Weiler, H. Huebl, and S. T. B. Goennenwein, Temperature-dependent magnetic damping of yttrium iron garnet spheres, *Phys. Rev. B* **95**, 214423 (2017).
- [71] M. A. Nielsen, A simple formula for the average gate fidelity of a quantum dynamical operation, *Physics Letters A* **303**, 249 (2002).
- [72] M. Kjaergaard, M. E. Schwartz, J. Braumüller, P. Krantz, J. I.-J. Wang, S. Gustavsson, and W. D. Oliver, Superconducting qubits: Current state of play, *Annual Review of Condensed Matter Physics* **11**, 369 (2020).
- [73] C. Wang, X. Li, H. Xu, Z. Li, J. Wang, Z. Yang, Z. Mi, X. Liang, T. Su, C. Yang, G. Wang, W. Wang, Y. Li, M. Chen, C. Li, K. Linghu, J. Han, Y. Zhang, Y. Feng, and H. Yu, Towards practical quantum computers: transmon qubit with a lifetime approaching 0.5 milliseconds, *npj Quantum Information* **8** (2022).
- [74] A. Place, L. Rodgers, P. Mundada, B. Smitham, M. Fitzpatrick, Z. Leng, A. Premkumar, J. Bryon, A. Vrajitoarea, S. Sussman, G. Cheng, T. Madhavan, H. Babla, H. Le, Y. Gang, B. Jaeck, A. Gyenis, N. Yao, R. Cava, and A. Houck, New material platform for superconducting transmon qubits with coherence times exceeding 0.3 milliseconds, *Nature Communications* **12** (2021).
- [75] M. D. Hutchings, J. B. Hertzberg, Y. Liu, N. T. Bronn, G. A. Keefe, M. Brink, J. M. Chow, and B. L. T. Plourde, Tunable superconducting qubits with flux-independent coherence, *Phys. Rev. Appl.* **8**, 044003 (2017).
- [76] A. Blais, A. L. Grimsmo, S. M. Girvin, and A. Wallraff, Circuit quantum electrodynamics, *Rev. Mod. Phys.* **93**, 025005 (2021).
- [77] J. Johansson, P. Nation, and F. Nori, Qutip: An open-source python framework for the dynamics of open quantum systems, *Computer Physics Communications* **183**, 1760 (2012).
- [78] P. Krantz, M. Kjaergaard, F. Yan, T. P. Orlando, S. Gustavsson, and W. D. Oliver, A quantum engineer's guide to superconducting qubits, *Applied Physics Reviews* **6**, 10.1063/1.5089550 (2019).
- [79] One could attempt to use flux-driving in order to increase the effective coupling strength, choosing ω_{ac} close to the magnon frequency. However, flux-driving also changes the coupling strengths g_1 and g_2 , as will be shown in the next section. These new coupling strengths are typically lower than their non-driven equivalents. Ultimately, the fidelity values including driving turned out to be lower than without driving.
- [80] U. Vool, A. Kou, W. C. Smith, N. E. Frattini, K. Serniak, P. Reinhold, I. M. Pop, S. Shankar, L. Frunzio, S. M. Girvin, and M. H. Devoret, Driving forbidden transitions in the fluxonium artificial atom, *Phys. Rev. Appl.* **9**, 054046 (2018).
- [81] M. F. Gely, M. Kounalakis, C. Dickel, J. Dalle, R. Vatré, B. Baker, M. D. Jenkins, and G. A. Steele, Observation and stabilization of photonic fock states in a hot radio-frequency resonator, *Science* **363**, 1072 (2019).